JOURNAL OF GEOPHYSICAL RESEARCH, VOL. 102, NO. D18, PAGES 21,867-21,890, SEPTEMBER 27, 1997

Microwave land surface emissivities estimated from SSM/I observations

Catherine Prigent [1]
Département de Radioastronomie Millimétrique, CNRS, Observatoire de Paris, France

William B. Rossow
NASA Goddard Institute for Space Studies, New York, New York

Elaine Matthews
Center for Climate System Research, Columbia University, NASA Goddard Institute for Space Studies, New York, New York

Abstract. Microwave emissivities of land surfaces are estimated from special sensor microwave/imager (SSM/I) observations by removing the contributions from the atmosphere, clouds, and rain using ancillary satellite data (International Satellite Cloud Climatology Project (ISCCP) and TIROS Operational Vertical Sounder (TOVS) products). In the first step, cloud-free SSM/I observations are isolated with the help of collocated visible/infrared satellite observations (ISCCP data). The cloud-free atmospheric contribution is then calculated from an estimate of the local atmospheric temperature-humidity profile (TOVS retrieval). Finally, with the surface skin temperature derived from IR observations (ISCCP estimate), the surface emissivity is calculated for all the SSM/I channels. As an exploration the method is applied to the SSM/I data for four months in 1991 within the Meteosat observation area. The magnitude and fluctuations of the atmospheric contributions are estimated along with the effect of surface temperature variations. Correspondences between geographical and seasonal patterns of the emissivities and topography, vegetation, flooding, and snow cover are analyzed. The potential for using microwave emissivities to monitor vegetation phenology and surface properties at regional and continental scale is investigated, and the possibility of retrieving atmospheric parameters (water vapor content, cloud liquid water path, and precipitation) over land is discussed.

1. Introduction

Global satellite microwave observations have been available for about 20 years, but large-scale studies over land surfaces have been limited. The reasons given are the coarse spatial resolution of the microwave measurements as compared to the spatial variability of the land surface and the complex interaction between the cloudy atmosphere and the underlying surface. The field of view of satellite microwave measurements is more compatible with the dimensions associated with atmospheric and oceanic variations, so most efforts have concentrated on atmospheric studies over ocean or studies on the ocean itself. Nevertheless, estimating land surface emissivities from satellite microwave measurements is of major interest for two main reasons.

First, if the surface contribution to microwave radiances could be determined accurately enough, then microwave retrievals of cloud liquid water and precipitation, now performed only over ocean, might be extended to land areas. The ocean surface is radiatively "cold" in the microwave regions because an emissivity of around 0.5 reduces the surface brightness temperature so that atmospheric phenomena appear with good contrast against this cold background. Moreover, the results are much less sensitive to errors in specifying ocean surface properties [*Lin and Rossow*, 1994; *Prigent et al.*, 1997]. Atmospheric parameter retrieval over land is much more difficult because of the higher emissivity of land surfaces, so very few studies have been directed to this objective. In one of them, *Jones and Vonder Haar* [1990] proposed a methodology for detecting cloud liquid water above land from the special

[1]Now at Columbia University, NASA Goddard Institute for Space Studies, New York, New York.

Paper number 97JD01360.
0148-0227/97/97JD-01360$09.00

sensor microwave/imager (SSM/I) data: Prior to estimation of the cloud liquid water content, they estimate the surface emissivity with the help of coincident visible satellite observations in cloud-free areas. Their analysis was limited to a case study in Colorado. More recently, *Conner and Petty* [1996] suggest an analysis of the time variability of SSM/I radiances over land to help separate the surface and atmospheric contributions.

Second, land surface emissivities derived from microwave satellite measurements could be used to monitor variations of surface and vegetation properties at regional and continental scales. An extensive body of research has been directed toward a better understanding of the mechanisms responsible for the microwave emission of soil and vegetation, both from theoretical analysis and from small-scale field experiments (using hand-held, truck-mounted, or airborne sensors). A thorough review of these developments is presented by *Ulaby et al.* [1986]. However, most satellite studies have focused on the use of simple indices derived from linear combinations of microwave satellite measurements. The microwave vegetation index (MVI), for instance, is based on the polarization difference at 37 GHz: For each month, the 37 GHz polarization differences over time are ranked, and the second lowest value is kept to maximize the vegetation response and minimize the effects of soil wetness and clouds. The MVI has been used to monitor vegetation or flooding from scanning multichannel microwave radiometer (SSMR) and SSM/I observations [e.g., *Choudhury and Tucker*, 1987; *Choudhury*, 1988, 1989; *Tucker*, 1989, *Justice et al.*, 1989]. However, as noted by several authors [*Tucker*, 1989; *Prince and Choudhury*, 1989; *Justice et al.*, 1989; *Tucker*, 1992; *Kerr and Njoku*, 1993], atmospheric effects, especially cloud cover, may be responsible for a large part of the 37 GHz polarization difference, casting doubt on interpretation of the MVI (or other simple indices) solely in terms of surface properties. Nevertheless, small-scale experiments show that microwave emissivities are sensitive to soil and vegetation properties, so that one can reasonably anticipate that direct estimation of microwave surface emissivities globally may yield useful information about the land surface despite the low resolution of the satellite microwave observations.

The microwave signal emanating at the top of the atmosphere is the combination of the surface and atmospheric contributions, the microwave emission of the land surface itself being the product of its physical temperature and the surface emissivity. The surface emissivity depends on the surface composition (soil, vegetation, snow, wetness, etc.) and geometry (soil roughness, geometry of the vegetation canopy, topography, etc.). While the atmospheric contribution and the surface temperature may vary rapidly in time for a given location, one can expect rather slow variations of the surface emissivity, mainly related to the vegetation cycle, except for snow and rainfall, which can cause significant modifications of the emissivity. In this study we start by assuming that the time variability of surface emissivities is small compared to the atmospheric variability on the scale of 1 month, and we retrieve monthly averages of the land surface microwave emissivities from the SSM/I observations by removing the contributions of clouds, rain, and the atmosphere using ancillary satellite observations. The International Satellite Cloud Climatology Project (ISCCP) analysis is used to detect the presence of clouds and to determine the variations in surface temperature that also affect microwave radiation. The analysis method is described, along with the satellite data used, in section 2. In this exploratory study, results are presented for 4 months in 1991 for the area covering Africa and large portions of Europe and western Asia (section 3). A sensitivity analysis is conducted to characterize the time variability of the emissivities during a month and from month to month. Correspondences between microwave emissivities and surface characteristics (topography, vegetation, inundation, and snow cover) are analyzed to explore the potential of microwave observations for monitoring vegetation phenology and other surface properties (section 4). Section 5 summarizes this study and outlines the possible uses of microwave land emissivities.

2. Methodology and Data

2.1. Principles

Over a flat lossy surface, the integrated radiative transfer equation for a non scattering plane-parallel atmosphere can be expressed in terms of brightness temperature for each orthogonal polarization P (P stands for horizontal, H, or vertical, V):

$$TbP = Tsurf \times emisP \times e^{-\tau(0,H)/\mu} + Tatm\_down \times (1 - emisP) * e^{-\tau(0,H)/\mu} + Tatm\_up \quad (1)$$

$$TbV - TbH = (Tsurf - Tatm\_down) \times e^{-\tau(0,H)/\mu} \times (emisV - emisH) \quad (2)$$

with

$$Tatm\_down = \int_0^H T(z)\alpha(z)e^{-\tau(0,z)/\mu}dz$$

and

$$Tatm\_up = \int_0^H T(z)\alpha(z)e^{-\tau(z,H)/\mu}dz.$$

TbP is the brightness temperature measured by the satellite for polarization P; $Tsurf$ is the surface "skin" temperature; $emisP$ is the surface emissivity for polarization P; $\mu = \cos(\theta)$, θ being the incident angle on the surface; $\alpha(z)$ is the atmospheric absorption by gases at altitude z; $T(z)$ is the atmospheric temperature at altitude z; and $\tau(z_0, z_1) = \int_{z_0}^{z_1} \alpha(z)dz$ is the atmospheric opacity from z_0 to z_1.

These equations lead to

From (1)

$$emisP = \frac{TbP - Tatm\_up - Tatm\_down \times e^{-\tau(0,H)/\mu}}{e^{-\tau(0,H)/\mu} \times (Tsurf - Tatm\_down)} \quad (3)$$

From (2)

$$emisV - emisH = \frac{TbV - TbH}{e^{-\tau(0,H)/\mu} \times (Tsurf - Tatm\_down)} \quad (4)$$

At SSM/I frequencies, the radiation emanates from only a thin surface layer of bare soil and water (the penetration depth is of order of the wavelength in soil and less for water [*Choudhury*, 1993]) with the following consequences: There is no volume scattering, the surface temperature is the skin temperature, and for flat surfaces the reflection is quasi-specular. However, volume scattering is involved in the cases of vegetation or snow cover, since the microwave radiation can arise from below and within the canopy or snow layer. When the terrain is rough on scales between the radiation wavelength and the size of the field of view, the surface acts as a set of scattering facets with a complex distribution of orientations. In these cases (1) to (4) involve some "effective" emissivity and temperature, aggregated over the depth of penetration and the field of view of the satellite instrument. These parameters correctly determine the observed radiation, but they are complicated functions of he actual distribution of surface properties. See *Ulaby et al.* [1986] for a review of the emission behavior of land surfaces.

Our method consists of solving the radiative transfer equation (3) for the surface emissivity for each SSM/I channel using ancillary data to specify the atmospheric and other surface parameters. We make use of a combination of SSM/I observations collocated with nearly coincident ISCCP products and daily TIROS Operational Vertical Sounder (TOVS) retrievals. In the first step, cloudy observations are eliminated, with the help of visible/infrared satellite observations (ISCCP data). The cloud-free atmospheric contribution is then calculated from an estimate of the atmospheric temperature and humidity profiles in the area (TOVS retrievals). Finally, with the surface skin temperature derived from IR observations (ISCCP data), the surface emissivity is calculated from (3).

2.2. Satellite data

The Defense Meteorological Satellite Program satellites (DMSP) observe the Earth twice daily from near-polar, circular, Sun-synchronous orbits. The orbital period is 102 min and the local time for the ascending equatorial crossing is 0612. The SSM/I instruments on board these satellites sense the atmospheric and surface emissions at 19.35, 22.235, 37.0, and 85.5 GHz with both horizontal and vertical polarizations, except for 22 GHz, which is vertical polarization only [*Hollinger et al.*, 1987, 1990]. The observing incident angle on the Earth is close to 53°, and the elliptical fields of view decrease in size proportionally with frequency, from 43×69, 40×50, and 28×37 to 13×15 km for 19.35, 22.235, 37.0, and 85.5 GHz, respectively. An instrument evaluation has been performed by *Hollinger et al.* [1990]. The SSM/I data from the F10 DMSP satellite have been obtained from Remote Sensing Systems [*Wentz*, 1988].

In the ISCCP data, cloud parameters and related quantities are retrieved from visible ((VIS) ~0.6 μm wavelength) and infrared ((IR) ~11 μm wavelength) radiances provided by the set of polar and geostationary meteorological satellites [*Rossow and Schiffer*, 1991]. The ISCCP data set is used not only to discriminate clear and cloudy scenes but also to estimate surface skin temperature. The pixel level data set (the DX data set) is used for its resolution of about 30 km and its sampling interval of 3 hours. The cloud detection scheme is described by *Rossow and Garder* [1993a] and evaluated by *Rossow and Garder* [1993b]. A detailed description of the ISCCP data is provided in *Rossow et al.* [1996]. In the ISCCP analysis the surface skin temperature is retrieved from clear IR radiances using the TOVS products to specify the atmospheric temperature and humidity profiles. Validation of the ISCCP land surface temperature is indirect since there are few systematic measurements of the land skin temperatures. *Rossow and Garder* [1993b] show that the ISCCP sea surface temperatures are in excellent agreement with other measurements: The local uncertainty of about 2 K combines errors in cloud detection, in the satellite radiance calibration, in the atmospheric temperature and humidity used in the retrieval, in the radiative transfer model treatment of the water vapor absorption, in the assumption of unit surface emissivity (instead of a value of about 0.98), and in the effect of real differences between the skin and bulk surface temperatures. Thus the uncertainties of land surface temperatures associated with these same factors (cloud detection, correcting for the atmosphere, and radiance calibration) are about the same magnitude, 2 K. Two other sources of surface temperature uncertainty that are more important over land are associated with much larger diurnal and rapid synoptic temperature variations and with cloud radiative effects. *Rossow and Garder* [1993a, b] show how the ISCCP analysis successfully separates these two types of variations and confirm the accuracy of individual surface temperature variations to within about 4 K. Systematic cloud-induced changes in surface radiative heating mean that the ISCCP surface temperature values include a "clear sky" bias: In summer average ISCCP surface temperatures will be systematically higher than the true mean temperatures, and in winter they will be lower than the true mean temperatures [*Rossow et al.*, 1989]. The magnitude of these biases is dependent on the average cloud cover and the sensitivity of the surface temperatures to changes in surface radiation. Fortunately, the biases are limited because these two characteristics are correlated: Where surfaces are less vegetated, drier, and therefore more sensitive, there is generally much less cloud cover; where cloud cover is

more persistent, the land surfaces are generally more vegetated, moister and, less sensitive. Although this problem will cause errors in attempts to retrieve cloud properties from microwave measurements over land, in the present case we use clear scenes to retrieve the microwave properties of the land, eliminating the effects of the bias. Another source of error in the ISCCP land surface temperatures comes from use of unit emissivity in the retrieval. The IR emissivity of various types of land surface materials is generally >0.9 mostly ≥0.95, varying between lower values for bare, dry soils and rock to higher values close to unity for vegetated areas [*Salisbury and D'Aria*, 1992a and references therein]. The consequent reduction of the radiation upwelling from the surface at a wavelength ~11 μm is equivalent to an underestimate of the temperature by, at most, 6-8 K [cf. *Ottle and Stoll*, 1993], generally ≤4 K for most materials. However, the temperature retrieval bias is reduced by 25-50% because the reduction in upwelling emission is partially offset by surface radiation of downwelling atmospheric IR emission. Although there is systematic variation of the IR emissivity from place to place because of changing surface properties, the time variability of the IR emissivity, caused by changes in the soil moisture [*Salisbury and D'Aria*, 1992b] or vegetation conditions [*Salisbury and D'Aria*, 1992a], is constrained to a very small range. We estimate that the IR emissivity variability is generally ≤0.03, which is equivalent to a spurious temperature variability of ≤2 K, well within the 4 K uncertainty associated with synoptic variations.

The daily atmospheric profiles used here are extracted from the TOVS system as gridded by ISCCP [*Rossow et al.*, 1996]. The TOVS system includes the high-resolution infrared radiation sounder (HIRS2), the stratospheric sounding unit (SSU), and the microwave sounding unit (MSU). The ISCCP TOVS data set includes nine layer-mean temperatures and precipitable water for five layers (middle and lower troposphere) at a spatial resolution of approximately 2.5°in latitude and longitude. The estimated uncertainty of the temperature retrievals is 2-3 K and 25-30% for the water vapor retrievals. Although the TOVS products are originally derived from two polar orbiters that can produce up to four atmospheric profiles a day, only one sounding per day usually contains the complete information (temperature and humidity). Neglecting the time of day in the processing of the temperature and profile humidity can yield additional errors in temperature and humidity in the lower layers of the atmosphere.

2.3. Practical Considerations

This exploratory study is limited to the region covered by the Meteosat geostationary satellite region, Africa, Europe, and western Asia, that encompasses a wide range of land surface types. To compare products at the same location over a month, the fixed map projection of the ISCCP Meteosat product is used [*Rossow et al.*, 1996], corresponding to a spacing of 25-30 km near the center of the Meteosat view. This grid spacing is fully compatible with the SSM/I observations which are also sampled at 25 km.

For each month the following procedure is applied. For each SSM/I pixel (day and night) within the Meteosat region, the collocated ISCCP DX Meteosat pixels are selected from the two DX images that bracket the SSM/I overpass time. Considered further are only SSM/I pixels that correspond to ISCCP pixels that are both clear or have only high clouds (cloud top temperature <260 K) with an optical thickness less than 1. High and thin ice clouds (i.e. thin cirrus) can be tolerated because of their negligible effect at SSM/I frequencies. In areas of persistent cloudiness such as tropical land areas covered by thin cirrus or low broken cumulus, tolerating thin cirrus in the scene helps increase the number of emissivity retrievals without degrading the accuracy of the retrievals (see section 3.4 for a discussion). SSM/I pixels with excessively low or high brightness temperatures (usually occurring together in a scan line) are excluded. At the time of SSM/I overpasses at these latitudes (close to sunrise and sunset up to mid-latitude), rapid changes of the surface temperature are observed, for example, up to 30 K over the desert in 3 hours. Selecting the closest-in-time Meteosat image to derive the surface temperature can produce large errors in the emissivity retrieval. Therefore a linear interpolation between the two ISCCP surface temperature estimations to the precise time of the SSM/I overpass is calculated. Using the closest TOVS profile (in time and space) and the MPM 93 model [*Liebe et al.*, 1993] for gaseous absorptions, the cloud-free atmospheric contribution is calculated for each SSM/I frequency. Equation (3) is then solved for the emissivity of each SSM/I frequency and polarization. For each ~30×30 km cell, the average and standard deviation of the emissivity is calculated for each month for each channel.

3. Results

Within the Meteosat observation area, the F10 SSM/I data have been processed for March, July, October, and December 1991, covering the annual vegetation cycle.

3.1. Emissivity Maps

Maps of retrieved emissivities at 19 and 85 GHz for vertical and horizontal polarizations are presented for October 1991 (Plates 1a and 1b). The polarization differences are also shown for these two frequencies (Plate 1c). The topography (the Global 10' elevation data from the U.S. Navy, 1984) and the vegetation classification map [*Matthews*, 1983] are displayed for the same region (Plates 2 and 3). Matthews' vegetation classification has been compiled from a large number of published sources. The vegetation data distinguishes 30 classes, which are grouped into 10 classes for this study as indicated in Table 1.

Regions of bare soil and rock (northern Africa, Arabian Peninsula, southwestern Africa) show low emissivities at horizontal polarization (Plates 1a and 1b, right panels) and high polarization differences (Plate 1c) compared to vegetated areas. At this spatial scale (~30×30 km), bare soils act as a smooth surface, producing high polarization differences associated with qua-

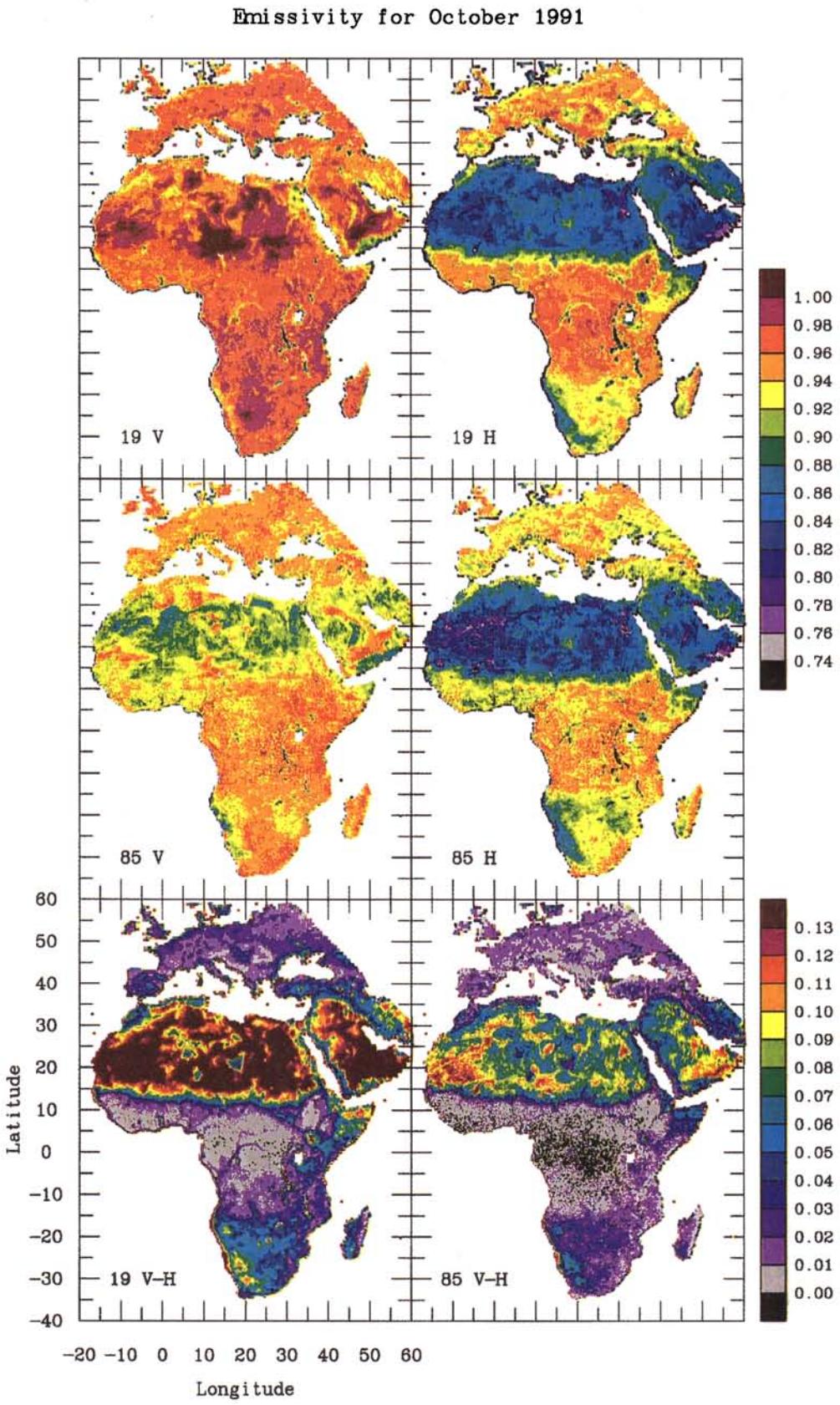

Plate 1. (a) Retrieved emissivities at 19 GHz for both polarizations for October 1991. (b) same as Plate 1a but at 85 GHz. (c) Emissivity polarization differences (emisV-emisH) at 19 and 85 GHz for the same month.

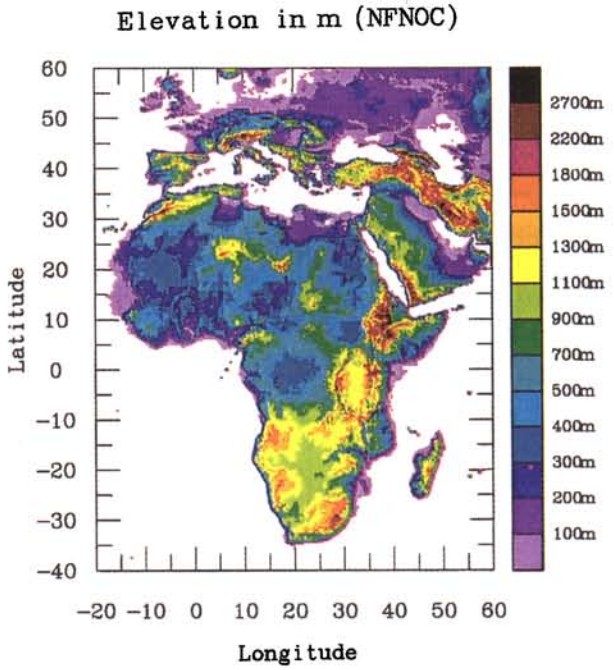

Plate 2. Topography map (extracted from the global 10-min elevation data from the U.S. Navy).

si-specular reflection. On the other hand, densely vegetated zones (the tropical rain forest for instance) exhibit high emissivities at horizontal polarization and low polarization differences because of scattering by the vegetation. For sparsely vegetated or unvegetated areas the polarization differences decrease with increasing topographic roughness. For example, the Sahara is associated with high polarization differences, but these differences decrease over the Tibesti or the Ahaggar mountain areas. Open water (lakes and rivers) exhibit very low emissivities with high polarization differences. The major river systems (Congo and Niger) and their associated wetlands appear clearly on the emissivity maps. In coastal areas where a substantial portion of the SSM/I pixel may include ocean, low emissivities are associated with high polarization differences (ocean in the "side lobes" of the SSM/I antenna pattern can also cause an underestimate of the microwave emission for coastal pixels). We illustrate these effects more specifically in section 4.

3.2. Sensitivity of the Estimated Emissivity

3.2.1. Sensitivity to the SSM/I instrumental errors. The sensitivity of the emissivity to errors in the measurement of brightness temperature is calculated from (3): It gives average values of 0.006/K at 22 and 85 GHz and 0.004/K at 19 and 37 GHz. The radiometric sensitivities of the SSM/I channels have been estimated by *Hollinger et al.* [1990] for the instrument on the F8 satellite, and the F10 radiometers are expected to have similar characteristics. With a typical value of 0.6 K the radiometric noise will induce only small uncertainties on the emissivity retrieval. On the other hand, the absolute calibration accuracy of the SSM/I, within ±3 K [*Hollinger et al.*, 1990], may contribute much more to the error budget. So far, calibration errors have not been definitively established.

Over the rainforest, differences between the vertical and horizontal polarizations at 85 GHz are often slightly negative (also seen to a smaller extent at 37 and 19 GHz), which was not expected and a calibration problem was at first suspected. *Neale et al.* [1990] also noticed that over land some pixels have brightness temperatures at 85GHz that are higher for the horizontal polarization than for the vertical polarization. However, *Matzler* [1990] measured a higher emissivity for horizontal than for vertical polarizations over an oat field during ripening. These features are explained in terms of scattering by prolate ellipsoids. Such an interpretation may also prevail at larger scale over the rainforest but would require accurate description of the vegetation canopy to be conclusive.

3.2.2. Sensitivity to the surface temperature. From (3) the sensitivity of the emissivity to errors in the surface temperature obtained from IR radiances can be written as follows

$$demis/dTsurf = -\frac{Tb - Tatm\_up - Tatm\_down \times e^{-\tau(0,H)/\mu}}{e^{-\tau(0,H)/\mu} \times (Tsurf - Tatm\_down)^2}.$$

The average sensitivity is estimated for July and October 1991 for a range of latitudes (Figure 1): The sensitivity varies somewhat with latitude and season but does not exceed 0.006/K. Thus, with an accuracy of the ISCCP surface temperature retrieval within 4 K, the r.m.s. uncertainty of emissivities caused by uncertainty in ISCCP surface temperature is about 0.024. The average differences in temperature between the two Meteosat overpasses that bracket the SSM/I observation time are also plotted in Figure 1. The large diurnal temperature variations in some areas, such as deserts

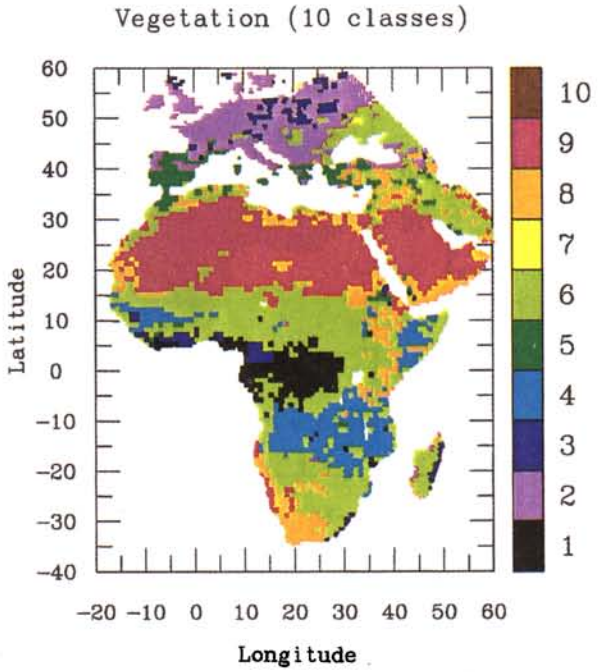

Plate 3. Vegetation map for 10 classes (see Table 1).

Table 1. Vegetation Types

Vegetation types			
30 Classes	10 Classes	Number of 30x30 km pixels in the Studied Area	Description
1	1	2432	tropical evergreen rain forest, mangrove
2	3	772	tropical/subtropical evergreen seasonal broadleaved forest
3	1	0	subtropical evergreen rainforest
4	3	0	temperate/subpolar evergreen rainforest
5	3	0	temperate evergreen seasonal broadleaved forest, summer rain
6	5	150	evergreen broadleaved sclerophyllous forest, winter rain
7	3	0	tropical/subtropical evergreen needleleaved forest
8	3	257	temperate/subpolar evergreen needleleaved forest
9	2	83	tropical/subtropical drought-deciduous forest
10	2	1131	cold-deciduous forest, with evergreens
11	2	336	cold-deciduous forest, without evergreens
12	8	92	xeromorphic forest/woodland
13	5	530	evergreen broadleaved sclerophyllous woodland
14	5	49	evergreen needleleaved woodland
15	4	3860	tropical/subtropical drought-deciduous woodland
16	4	0	cold-deciduous woodland
17	8	606	evergreen broadleaved shrubland/thicket and dwarf shrubland
18	8	18	evergreen needleleaved or microphyllous shrubland/thicket
19	8	151	drought-deciduous shrubland/thicket and dwarf shrubland/thicket
20	8	0	cold-deciduous subalpine/subpolar shrubland and dwarf shrubland
21	8	1899	xeromorphic shrubland/dwarf shrubland
22	7	12	arctic/alpine tundra/mossy bog
23	6	3408	tall/medium/short grassland with 10-40% tree cover
24	6	1821	tall/medium/short grassland with <10% tree or tuft-plant cover
25	6	5314	tall/medium/short grassland with shrub cover
26	6	603	tall grassland, no woody cover
27	6	310	medium grassland, no woody cover
28	6	520	meadow/short grassland, no woody cover
29	6	1	forb formation
30	9	10007	desert (bare soil)

The 30 vegetation classes are as defined by Matthews [1983]. The number of pixels covered by each vegetation type in the study area is indicated. The 10 class vegetation classification is also defined, in relation to the Matthews' original classification.

where the temperature can change by 30 K in 3 hours, would produce errors in the retrieved microwave emissivity as large as 0.18 without the interpolation to the precise time of the SSM/I observation.

About 6% of the emissivities at 19 GHz in the desert areas are slightly >1, which is not physical (Plate 1a). With the sensitivity of the 19 GHz V channel to surface temperature variations, -0.0035/K, an underestimate of surface skin temperature by at least 3 K would explain this effect. Such an underestimate would be produced by an IR emissivity of about 0.96 consistent with values for dry soils [*Salisbury and D'Aria*, 1992a].

3.2.3. Sensitivity to the atmospheric water vapor profile. The sensitivity of the emissivity retrieval to errors in the humidity profile is estimated by modifying the relative humidity in each layer of the atmospheric profile and calculating from (3) the corresponding error in the emissivity. The results are presented in Table 2 for the U.S. standard, tropical, and subarctic atmospheres. The 22 and 85 GHz channels show the highest sensitivity to errors in the water vapor profile, as expected, while the 19 and 37 GHz channels have lower sensitivities. The lower the emissivity, the higher the sensitivity to the water profile because of the reduced contribution of the surface to the measured radiance. For the estimated 30% uncertainty in TOVS water vapor amounts, the emissivity uncertainties at 19 and 37 GHz range from about 0.001 at higher latitudes to 0.02 at lower latitudes; the corresponding uncertainties at 22 and 85 GHz are from about 0.005 to 0.1. We return later (section 5) to the question of whether the column water vapor abundance can actually be retrieved from SSM/I over land.

3.2.4. Sensitivity to the water vapor absorption model. In the microwave spectrum, water vapor and oxygen are the main atmospheric absorbers. The MPM93 gaseous absorption model [*Liebe et al.*, 1993] is adopted. In this model the H_2O and O_2 lines are included up to 1 THz and an empirical H_2O continuum derived from laboratory measurements is added. The

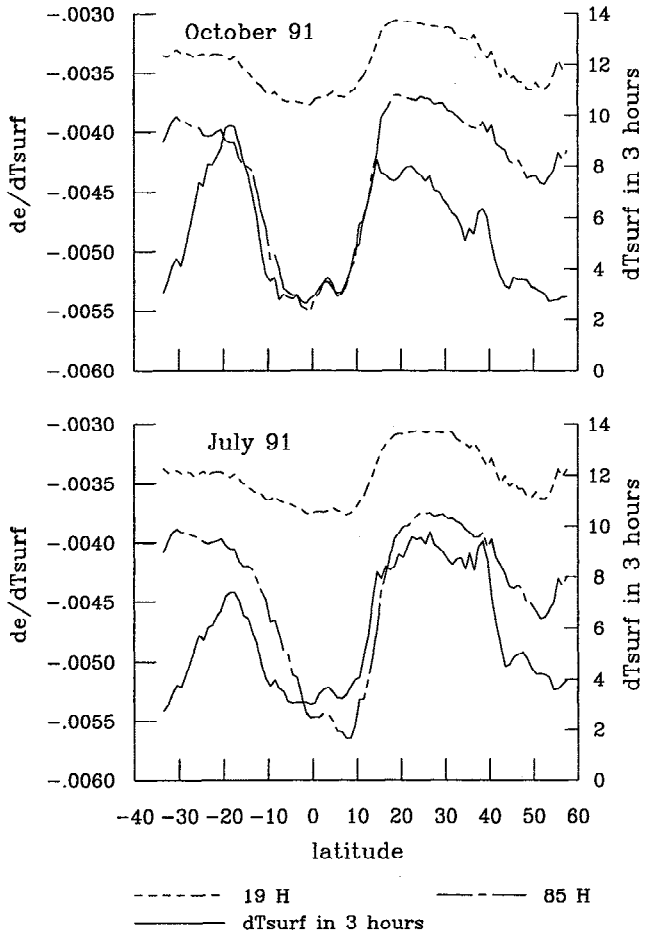

Figure 1. Sensitivity of the retrieved emissivities to changes in surface temperatures at 19 and 85 GHz for the horizontal polarization for July and October 1991. The zonal mean values are presented. The zonal mean differences in surface temperatures between two Meteosat overpasses (3 hours) are also plotted.

behavior of the H_2O absorption in the gaps between the lines is still a debatable point and theoretical and experimental efforts are still being carried out to increase the accuracy of the estimation of this so-called continuum. Depending on the frequency and the atmospheric condition, up to 10% error in the H_2O continuum absorption may occur [*Han et al.*, 1994; *English et al.*, 1994; *Snider et al.*, 1995]. The impact of a 10% decrease of the continuum absorption on the retrieved emissivity is estimated for three different atmospheres and is generally comparable to the effect of the water vapor uncertainty in the tropics and smaller at higher latitudes (Table 3). The sensitivity to the water vapor absorption model and the sensitivity to the water vapor profile follows similar trends: The higher the frequency, the higher the sensitivity, with an increased sensitivity with decreasing surface emissivities.

3.3. Fluctuations of the Atmospheric and Surface Contributions

To estimate the cloud and rain contributions to the SSM/I observations, the time variability of all SSM/I measurements over a month are compared with only the cloud-free SSM/I measurements (i.e. when the two Meteosat observations that bracket the SSM/I observation are both cloud-free or contain only high and thin ice clouds). The standard deviation of Tb in cloud-free pixels and for all the SSM/I pixels (clear and cloudy) are calculated over a month and the zonal means of differences of standard deviations are plotted in Figure 2. The zonal average number of all SSM/I observations along with the zonal average number of cloud-free situations are also shown. At 85 GHz, which is the channel most sensitive to the presence of liquid water, most of the time variability is associated with clouds and rain in zones where they are prevalent (e.g., the tropics and midlatitudes). At 19 GHz, which is the channel least sensitive to liquid water, little of the temporal variability is explained by clouds and rain. The high time variability of the 19 and 85 GHz above 35°N for both clear and cloudy pixels is due to the coast effects: For a given latitude above 35°N a large proportion of the pixels are situated on the coasts and have a high standard deviations (see below Figure 3 and the corresponding explanation).

The influence of the high and thin clouds can be estimated by comparing the standard deviations of the 85 GHz channel (H polarization) when considering only the cloud-free pixels and when including high and thin clouds in the SSM/I fields of views. The ratio of the number of cloud-free pixels to the number of cloud-free plus high and thin cloud pixels has been calculated and shows that tolerating high and thin clouds increases the number of retrieved pixels by up to 20% in areas of

Table 2. Sensitivity of the Retrieved Emissivity to the Water Vapor Content in the Atmosphere (de/dWV in $(kg/m^2)^{-1}$) for Three Different Atmospheres, Three Different Emissivities, and Four SSM/I Frequencies

	Frequency, GHz			
e	19	22	37	85
		Subarctic [a]		
0.95	-.34e-3	-.84e-3	-.35e-3	-.15e-2
0.85	-.12e-2	-.33e-2	-.12e-2	-.52e-2
0.75	-.20e-2	-.57e-2	-.19e-2	-.89e-2
		U.S. Standard Atmosphere [b]		
0.95	-.21e-3	-.30e-3	-.21e-3	-.72e-3
0.85	-.10e-2	-.26e-2	-.99e-3	-.42e-2
0.75	-.18e-2	-.49e-2	-.17e-2	-.77e-2
		Tropical [c]		
0.95	-.26e-3	-.18e-3	-.32e-3	-.45e-3
0.85	-.11e-2	-.24e-2	-.13e-2	-.53e-2
0.75	-.19e-2	-.46e-2	-.23e-2	-.10e-1

[a] $Tsurf = 257K; WV = 4.3 kg/m^2$
[b] $Tsurf = 287K; WV = 14.3 kg/m^2$
[c] $Tsurf = 299K; WV = 40.4 kg/m^2$

Table 3. Sensitivity of the Retrieved Emissivity to the Water Vapor Absorption Model (difference in the retrieved emissivities for a 10% decrease in the water vapor continuum absorption) for Three Different Atmospheres, Three Different Emissivities and Four SSM/I Frequencies

	Frequency, GHz			
e	19	22	37	85
	Subarctic [a]			
0.95	.26e-4	.34e-4	.96e-4	.50e-3
0.85	.88e-4	.11e-3	.32e-3	.17e-2
0.75	.15e-3	.19e-3	.54e-3	.29e-2
	U.S. Standard Atmosphere [b]			
0.95	.50e-4	.57e-4	.17e-3	.71e-3
0.85	.23e-3	.29e-3	.83e-3	.42e-2
0.75	.41e-3	.53e-3	.15e-2	.76e-2
	Tropical [c]			
0.95	.19e-3	.18e-3	.66e-3	.12e-2
0.85	.76e-3	.94e-3	.27e-2	.12e-1
0.75	.13e-2	.17e-2	.48e-2	.22e-1

[a] $Tsurf = 257K; WV = 4.3kg/m^2$
[b] $Tsurf = 287K; WV = 14.3kg/m^2$
[c] $Tsurf = 299K; WV = 40.4kg/m^2$

persistent cloudiness (e.g., in the ITCZ), without a significant increase in the Tbs standard deviations for a month: The maximum increase is ~3 K for a few isolated pixels in the ITCZ, where the actual mismatch of ISCCP and SSM/I can occasionally allow for stronger cloud contamination of the SSM/I pixel.

To estimate the contribution of the cloud-free atmosphere alone to the observed microwave radiances, we calculate

$$\frac{Tb - Tsurf \times emis \times e^{-\tau(0,H)/\mu}}{Tb}.$$

Figure 3 shows this ratio averaged over July and October 1991 at each latitude. Only the pixels used in the estimation of the emissivities, that is, cloud-free pixels or pixels with high and thin clouds, are included. For a given frequency the vertical polarization is always a little less sensitive to the atmospheric contribution than is the horizontal polarization. The sensitivity to the atmosphere also follows frequency in the expected way. At 19 and 37 GHz, less than 15% of the measured clear-sky brightness temperatures is due to the atmosphere; the atmospheric contribution goes up to 50% over the desert in July at 22 and 85 GHz. The 19 GHz vertical polarization near 20°N shows a slightly negative contribution of the atmosphere because of an estimated emissivity larger than one in this area. Figure 3 also shows the zonal monthly mean surface temperatures versus latitude. In (1) with a low contribution from the atmosphere (i.e., low water vapor amounts) and a surface emissivity close to 1, a change in Tb is directly related to a change in surface temperature. This is also true for $TbV - TbH$. As a consequence, even if cloudy conditions are carefully avoided and the contribution of the cloud-free atmosphere to the $TbV - TbH$ values at 19 and 37 GHz is low, it is not possible to compare $TbV - TbH$ over long periods or from one area to another without accounting for surface temperature changes. The modulation of the signal by the surface temperature, which is highly variable in time and space, precludes direct comparisons of the $TbV - TbH$ values with vegetation-related parameters. This seriously limits the usefulness of the MVI.

After removing the effects of clouds, rainfall, atmospheric emissions and surface temperature variations, the remaining variability of the retrieved surface emissivities is quite small over a month. Figure 4 shows the

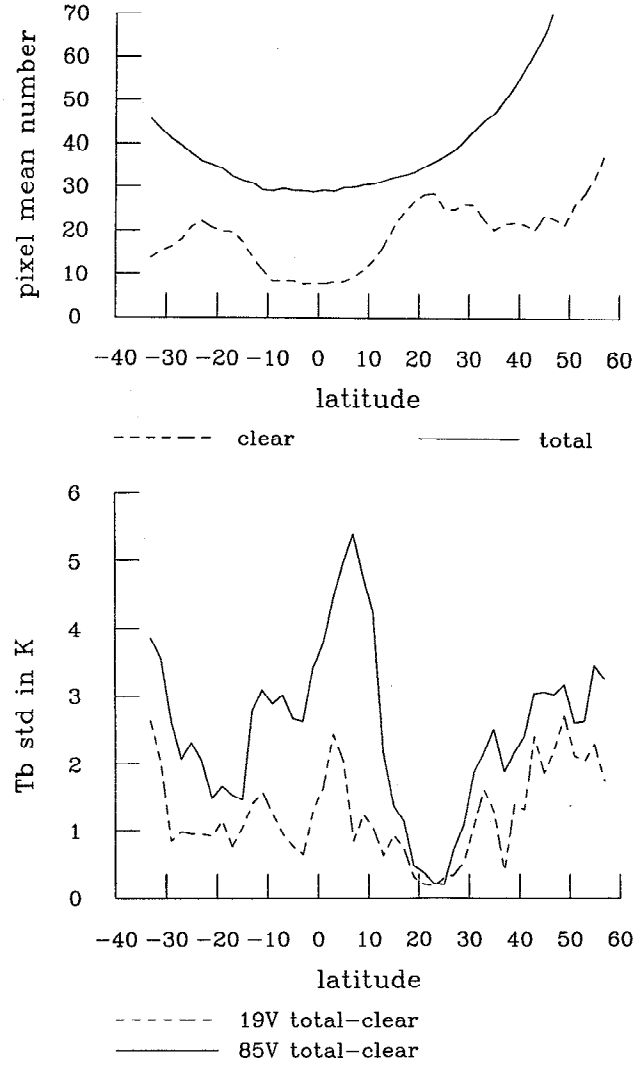

Figure 2. The standard deviation of all the SSM/I *Tbs* minus the standard deviation of the SSM/I *Tbs* for cloud-free pixels only, at 19 and 85 GHz (vertical polarization) for October 1991. The zonal mean values are presented. The zonal mean number of SSM/I overpasses is also shown, along with the zonal mean number of cloud-free overpasses for October 1991.

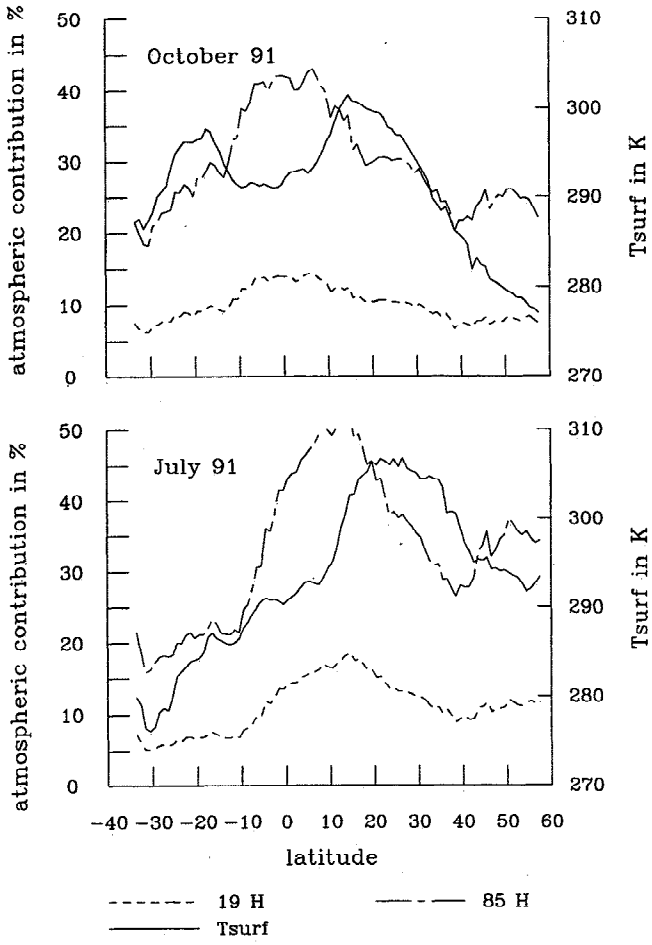

Figure 3. Zonal mean contribution of the cloud-free atmosphere to the total measured radiance. The results are presented at 19 and 85 GHz for horizontal polarization for July and October 1991. The zonal mean surface temperature is also plotted.

standard deviations of the retrieved emissivities at 19 and 85 GHz horizontal polarizations for October 1991. Histograms of the standard deviations of the emissivities for individual land points for October and July are presented in Figure 5. The mode values of the standard deviations never exceed 0.012, confirming our original hypothesis that the land surface emissivities are nearly constant over a month, despite large and complex spatial variability. Most of the observed day-to-day variability, which is caused by variations of the surface temperature and atmospheric properties, has been removed.

Nevertheless, the more sensitive the channel to the atmosphere, the larger the standard deviations of the emissivities, suggesting that there are still some residual errors associated with the atmosphere. Although surface temperature errors do not favor any particular channel, those errors in the ISCCP surface temperatures caused by errors in the TOVS atmospheric properties reinforce the direct effect of the atmospheric errors on the retrieved microwave emissivities. This effect is particularly evident over North Africa, where the 85 GHz horizontal polarizations shows much larger standard deviations (Figure 4) with obviously spurious square patterns that are related to the 2.5°×2.5° TOVS resolution. These areas of high 85 GHz emissivity standard deviations correspond to regions of very high standard deviations in the TOVS water vapor abundances but not to any notable features in the original SSM/I radiances. These problems in the TOVS data are caused, in part, by neglect of diurnal variations in the "first guess" surface air temperature used in the original analysis, which were based on assimilated surface temperature from the NCEP forecast model used at the time [cf. *Jin et al.*, 1996]. Moreover, use of once-per-day atmo-

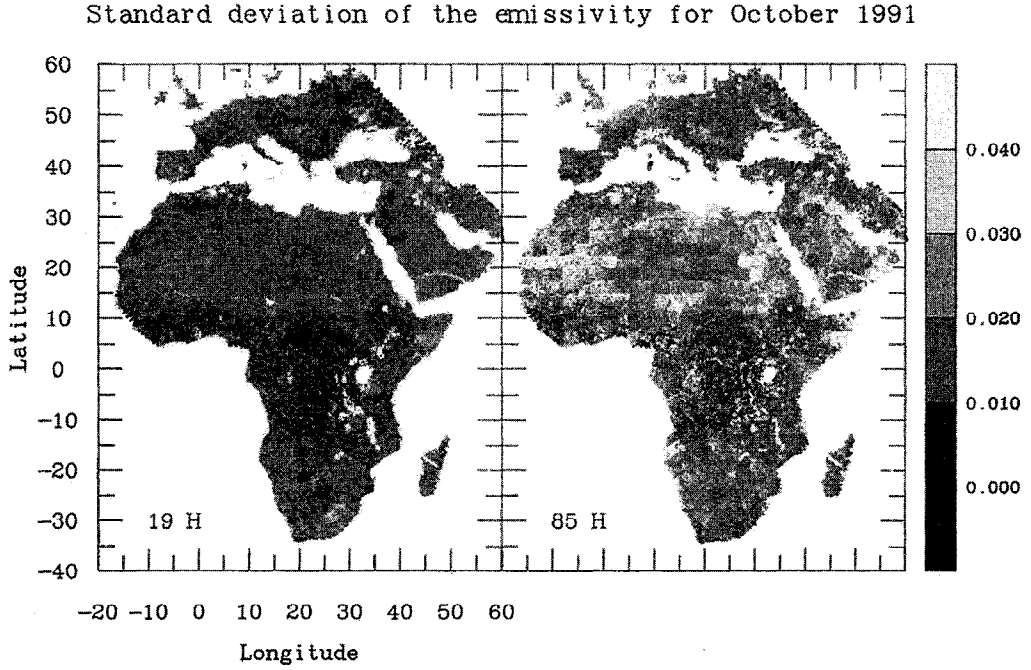

Figure 4. Standard deviations of the retrieved emissivities for 19 and 85 GHz horizontal polarizations for October 1991. Negative values mean that fewer than two pixels have been processed and standard deviation could not be calculated.

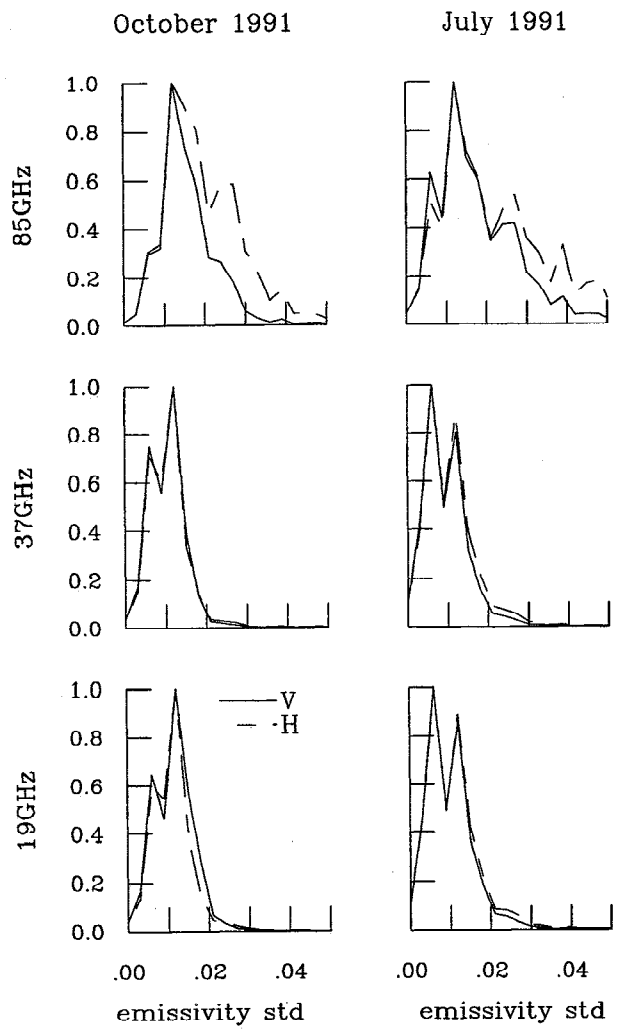

Figure 5. Histograms of standard deviations of retrieved emissivities for a month. The results are presented at 19, 37, 85GHz for both polarizations for July and October 1991.

spheric profiles neglects actual diurnal variations of the lower atmosphere. If we replace the TOVS data with assimilated water vapor fields from the NCEP/NCAR re-analysis, the square artifacts in the emissivity disappear.

Rivers, coasts and lake shores (i.e. land-water boundaries) are also associated with high standard deviations that can be interpreted as satellite navigation errors. These features are particularly obvious at 85 GHz: with a 13×15 km resolution, this channel is more sensitive to mislocation problems than the 19 GHz channel (43×69 km resolution).

The stringent constraint imposed with respect to cloudiness (no clouds or only high and thin clouds before and after the SSM/I overpass) limits the number of retrieved pixels but eliminates any sign of contamination by clouds. For a given area the number of retrieved pixels for a month varies from 0 in regions of persistent clouds to 80. The zonal mean number of retrieved pixels is plotted on Figure 2. Because of the orbit of the satellite and the scan pattern of the SSM/I, the number of satellite overpasses per month is lower at the equator and increases as one moves to the pole. In the inter tropical region between 10°S and 10°N, the average number of cloud-free overpasses falls to near 10. Portions of tropical land areas are completely covered by cirrus and low broken clouds for periods longer than a month. In our processing, tolerating additional types of optically thin clouds in the SSM/I field of view would increase the number of data points per month: While this might be acceptable for the lower frequency channels, it would certainly affect the 85 GHz channel, which is highly sensitive to low liquid water clouds [*Weng and Grody*, 1994; *Prigent et al.*, 1997]. Depending on the application and the frequencies used for it, cloud constraints can be optimized. Further tests must be carried out to determine the maximum cloud amount acceptable for each specific application and each channel without degrading the quality of retrieved emissivities.

Figure 5 summarizes the overall uncertainty of the land surface emissivities retrieved by our analysis: The day-to-day variability of the emissivities are generally <0.02 and typically about 0.01 which is about the error expected from uncertainties in the ISCCP surface temperature and the TOVS atmospheric properties. These distributions represent upper limits on the retrieval errors. The notable exceptions for 85 GHz are associated with larger errors in the TOVS water vapor abundances over Africa. This figure also confirms the hypothesis that land surface emissivities are nearly constant in time in most areas.

4. Correlation of Microwave Emissivities with Surface Properties

We now focus on the geographical and seasonal patterns of land surface microwave emissivities and argue that they can be represented by their correspondences with recognized variations in the topography, vegetation types, snow cover, and flooding because these emissivity changes are generally larger and more coherent that the estimated retrieval uncertainties (Figure 5). However, because we lack direct information about the surface emissivity at these relatively large spatial scales, our comparisons can only provide indirect support for our interpretations. In particular, we note some specific difficulties in relating the surface properties to our "effective" emissivity values. These same difficulties point, however, to the potential value of using such a combination of microwave and other satellite observations to study regional land surface variations: Further progress in understanding the microwave emission from land surfaces is facilitated by removing the confusing atmospheric effects on the microwave radiances with our approach.

4.1. Influence of Topography

Different roughness scales may be involved within a single field of view, from the small-scale roughness related to surface irregularities, small compared to the

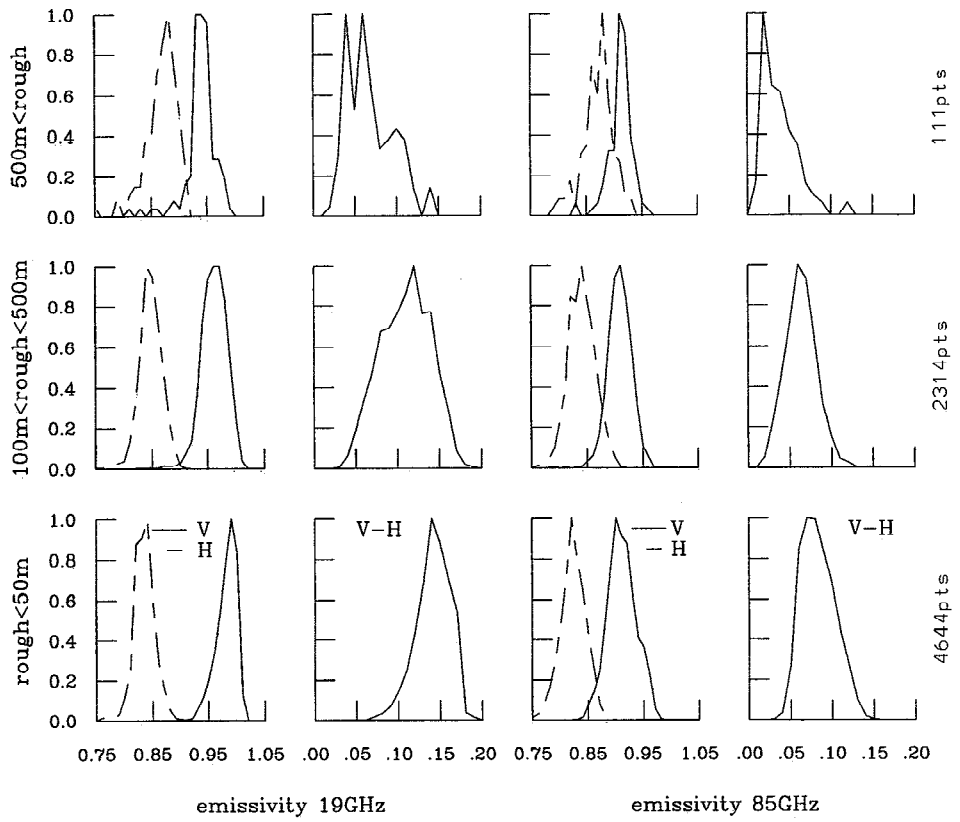

Figure 6. Histograms of emissivities at 19 and 85 GHz (both polarizations) for October 1991 over the north African desert for three ranges of large scale surface roughness. The number of pixels involved in each category is shown on the right of the figure.

wavelength, to the large-scale topographic effects. The effect of topography is to locally modify the viewing angle with respect to the horizontal and vertical polarizations as defined for a flat surface. Within a field of view, different surface slopes related to topography tend to mix the vertical and horizontal polarizations as defined relative to the mean flat surface. Thus with increasing topographic roughness, the reflection properties of the surface approaches a lambertian behavior.

In vegetated areas this feature is difficult to evaluate, first because the vegetation usually changes with the topography, and second because the emissivity difference in polarizations is already low. To closer examine the influence of the topography on the emissivity, the histograms of the emissivities are presented at 19 and 85 GHz, for the north African desert, for selected ranges of terrain roughness (Figure 6). The roughness at a point is measured as the standard deviation of the elevation of the terrain, on a 90x90 km square centered on this point.

As expected, Figure 6 shows that the difference of polarization decreases with increasing terrain roughness. The 19 GHz channel is more sensitive than the 85 GHz channel to the topography. In area of low roughness, the polarization difference is already smaller at 85 GHz because the higher the frequency, the larger the effect of the small scale roughness of the soil surface.

4.2. Correlation with Vegetation Phenology

Maps of emissivities at 19 GHz for both polarizations for March, July, and December are presented in Plate 4. Maps for October were presented in Plate 1a.

The Saharan/Arabian desert shows very high polarization differences as expected for quasi-specular surfaces. The sand fields of Mauritania (El Djouf), Niger (Tenere), and Libya appear with very high emissivities at vertical polarization. The sharp gradient southward of 15°N corresponds to the Sahelian transition between arid shrub grassland to more humid grassland with tree cover. The transition zone is broader in winter than it is in summer. In the grassland area in Southern Africa (see Plate 3), vegetation density declines during the southern hemisphere winter: The emissivity in 19 GHz horizontal polarization is lower as is the difference in polarizations. Woodland areas in southeastern Africa also exhibit changes in emissivities during the annual vegetation cycle. The polarization difference decreases over most of Europe in summer, where deciduous woodlands are present. However, in Spain, where the vegetation is dominated by sclerophyllous or arid evergreen woodlands (see Plate 3), the polarization difference does not change much during the year.

That the microwave emissivities of the denser vegetation types behave more like lambertian scatterers (small

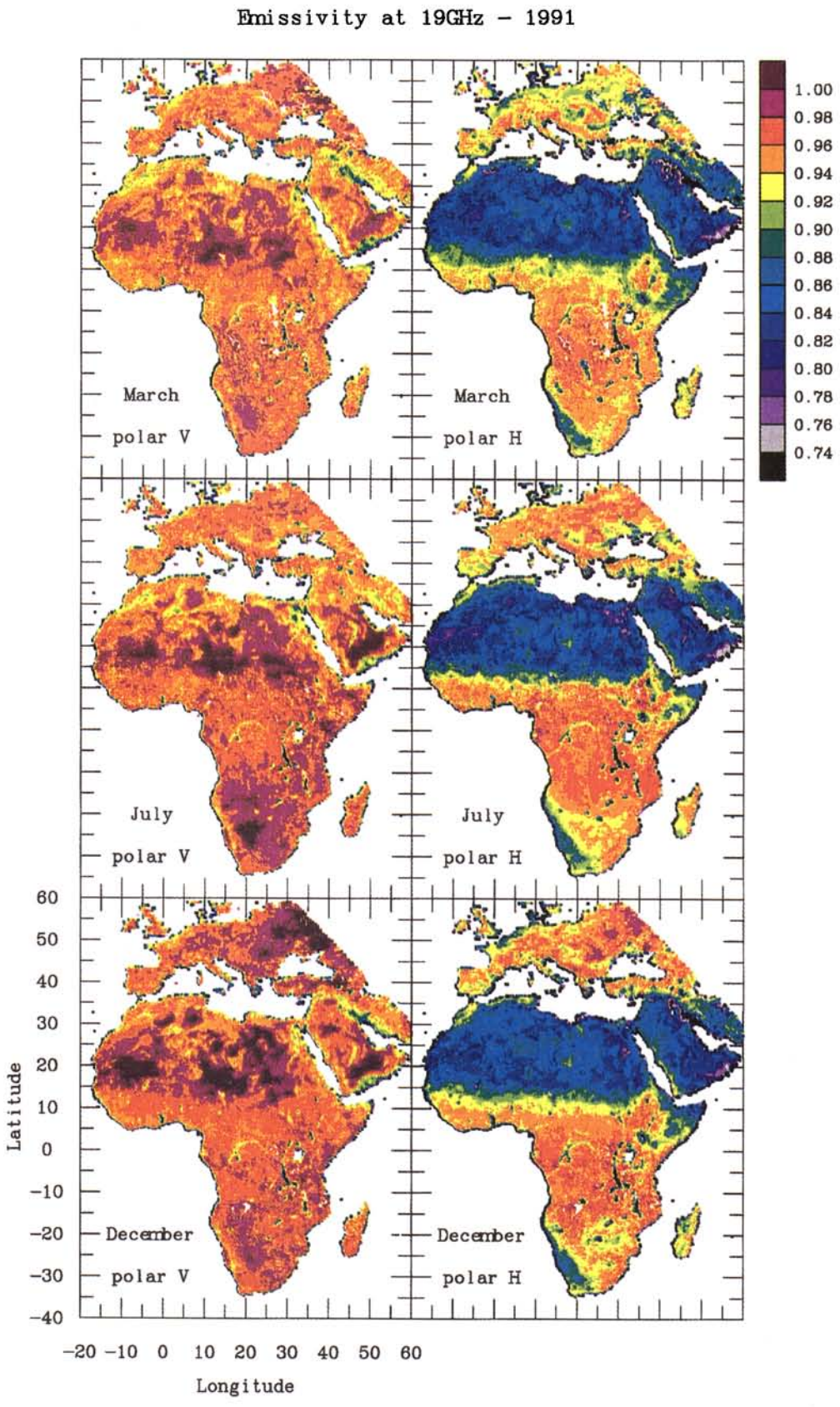

Plate 4. Emissivity maps at 19 GHz for March, July, and December 1991 for both polarizations. The map for October is presented in Plate 1a.

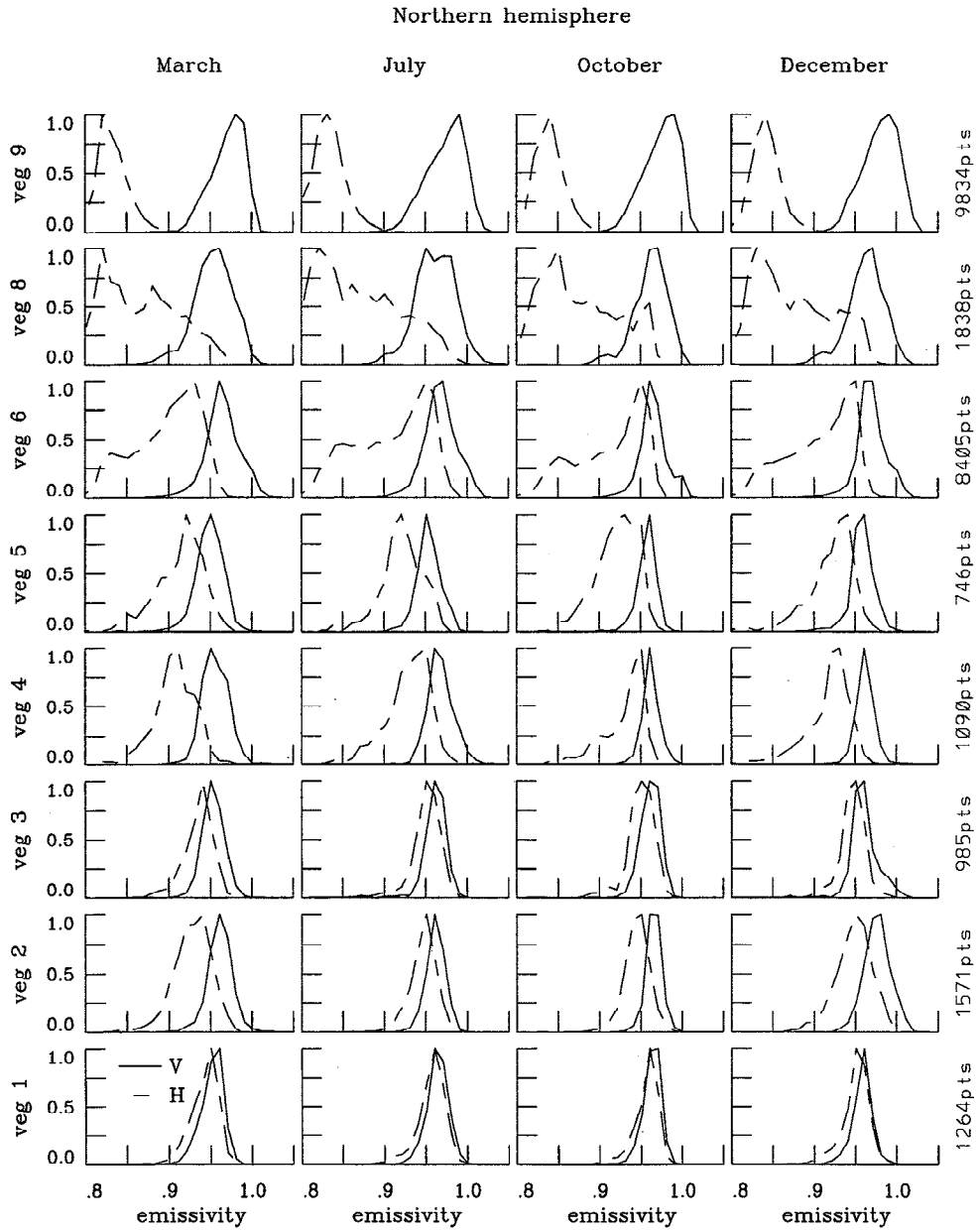

Figure 7a. Histograms of retrieved emissivities at 19 GHz (both polarizations) for the 10 vegetation types (see Table 1 for a description of the vegetation types). Results are presented for March, July, October, and December 1991 for the northern hemisphere. The number of pixels involved in each class is shown on the right of the figure.

polarization differences) means that a significant portion of the microwave arises from within the vegetation canopy. Since the temperature of the forest canopy can vary over its vertical extent (e.g., *Hall et al.*, [1992] show this effect even in grasslands), the IR skin temperature may differ systematically from, but vary together with, the average microwave emission temperature for forests. Whether the effects of differing penetration depths between different wavelengths of radiation can be detected and exploited deserves further study.

Histograms of 19 GHz emissivities are presented in Figures 7a and 7b for the 10 vegetation types (Table 1) for the four studied months separated by hemisphere. The classes that are underrepresented are omitted (see Plate 3). With decreasing biomass density (from class 1 to class 9), the horizontal polarization decreases, the vertical polarization increases, and the polarization difference increases in all months. Most histograms are well defined with only one mode (classes 2, 3, 5, and 9 in the southern hemisphere are disregarded because they are underrepresented). The widths of the histograms are much larger than are the standard deviations of the emissivities over the month at individual locations (see Figure 5): Dispersion in the histograms thus represents actual surface variability. Although covering a large area, the xeromorphic vegetation type (class 8)

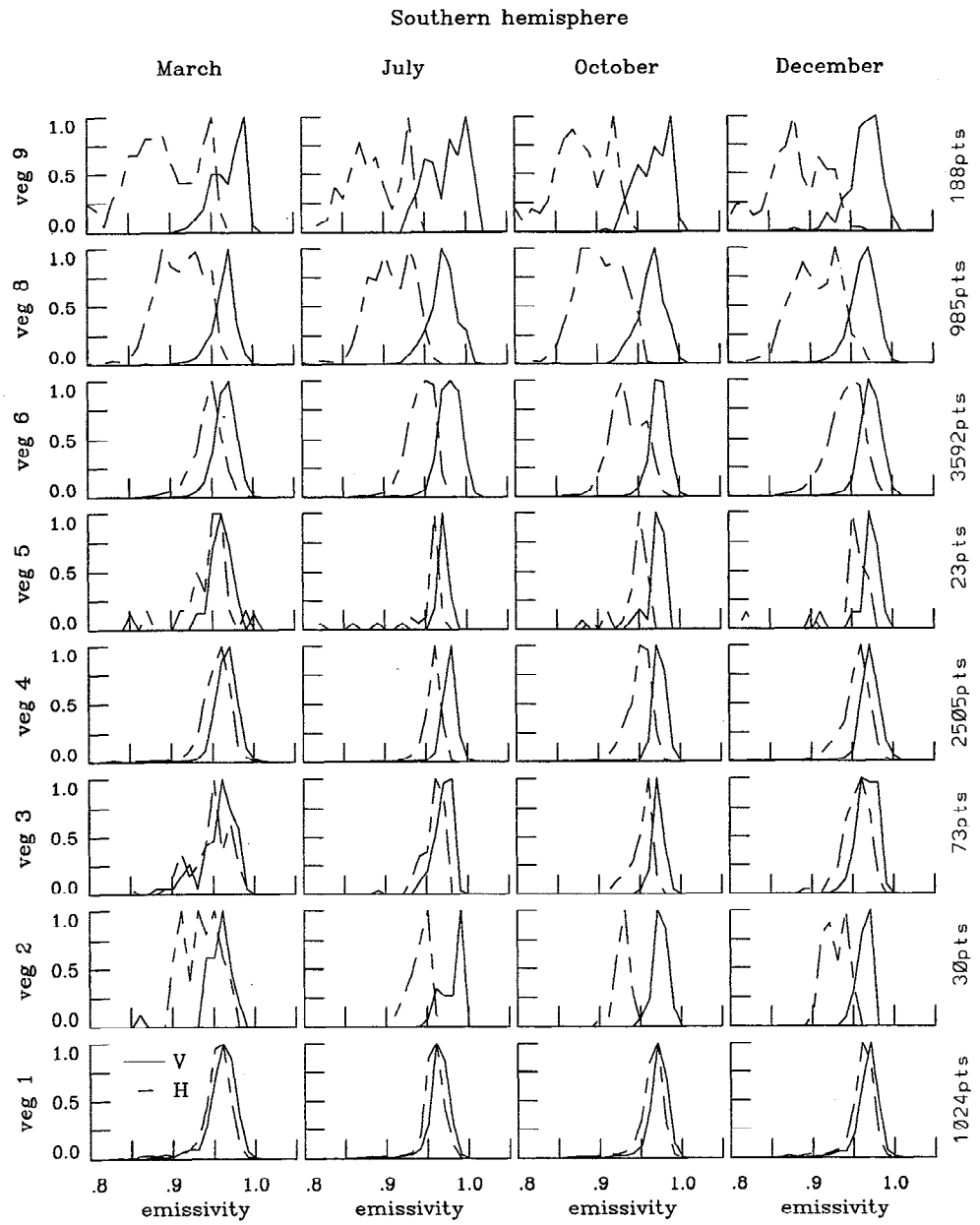

Figure 7b. Histograms of retrieved emissivities at 19 GHz (both polarizations) for the 10 vegetation types (see Table 1 for a description of the vegetation types). Results are presented for March, July, October, and December 1991 for the southern hemisphere. The number of pixels involved in each class is shown on the right of the figure.

does not have the same behavior in the two hemispheres and does not exhibit narrow distributions: Vegetation in these arid zones is not well defined and can encompass a very broad range of conditions [cf. *Matthews and Rossow*, 1987]. In the northern hemisphere the grassland histogram in horizontal polarization is also very broad, with a second peak corresponding to low emissivities. Comparison of Plates 3 and 4 shows that the desert-like emissivity signature in northern Africa extends slightly farther south than in the vegetation map, with a very gradual transition compared to the vegetation map. In addition, and more important, Iran has a desert-like emissivity in microwave, while the vegetation map indicates grassland. On NDVI maps (normalized vegetation index as derived from optical and visible AVHRR data), Iran also shows a desert-like behavior. While the sensitivity of the microwave emissivities to very sparse, arid vegetation is expected to be low, the vegetation classification may also have to be reexamined, particularly with respect to geographic transitions and recent changes.

Seasonal variations in emissivity are examined for the 10 vegetation classes at 19, 37, and 85 GHz for both polarizations and for the difference in polarizations. Figures 8a and 8b show monthly mean emissivities for the southern and northern hemispheres, respectively. For

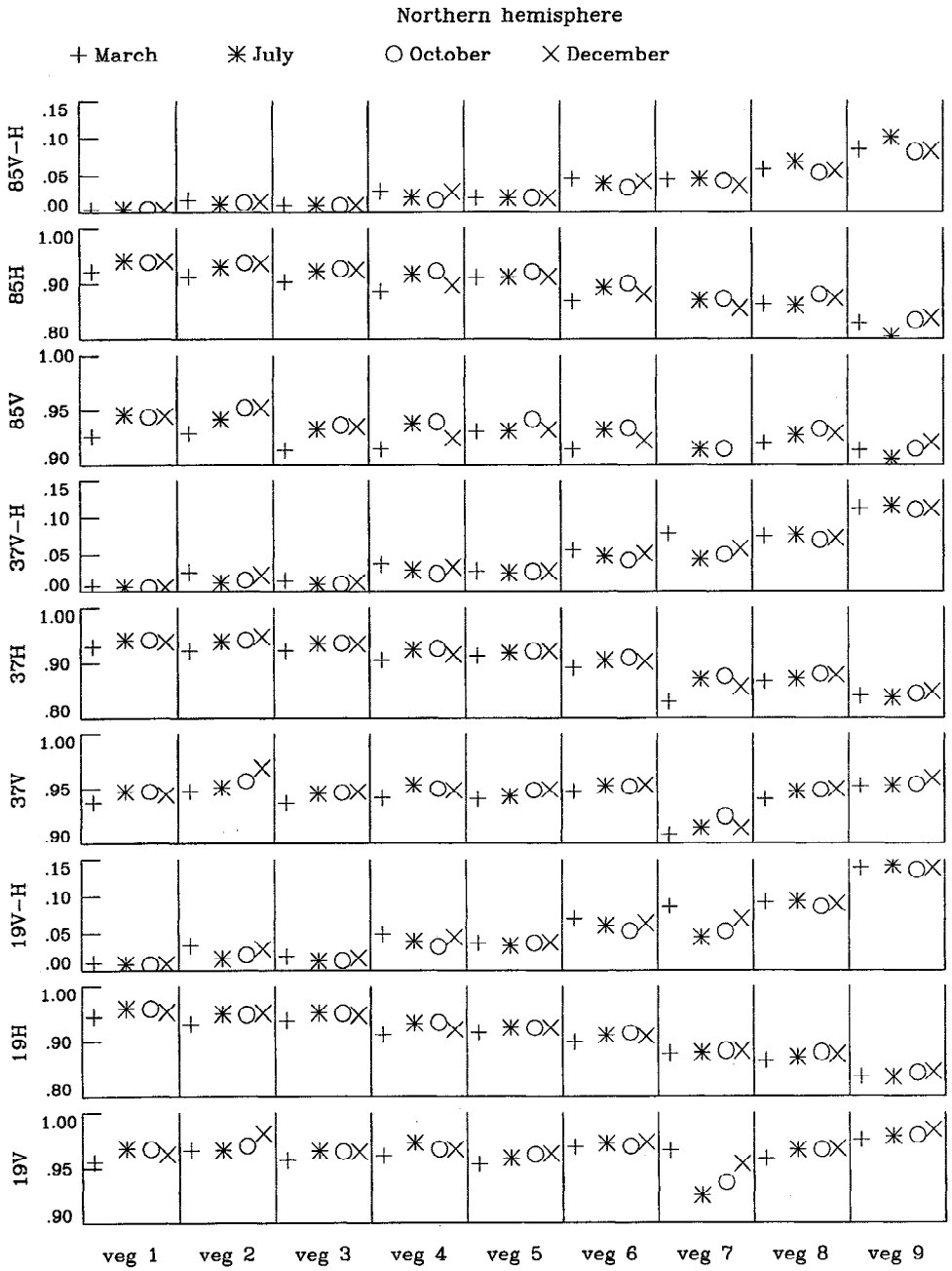

Figure 8a. Variations of the mean value of the emissivity at 19, 37, and 85 GHz (for both polarizations and difference in polarizations) for the four studied months and for the 10 vegetation types. Results are presented for the northern hemisphere.

each hemisphere, underrepresented classes are ignored (see Plate 3). The emissivities for vegetation classes exhibit similar variations with frequency. This property of the emissivity can be exploited to estimate the land emissivities at other microwave frequencies by interpolation. For instance, this result can be used for the Advanced Microwave Sounder Unit (AMSU), on board the new generation of TIROS-NOAA satellites: the prospect of AMSU processing calls for an estimate of the land surface emissivities around 60G Hz to aid retrieval of atmospheric profiles above land. However, emissivities show very different behavior with frequency under snow conditions, as can been seen for the northern hemisphere over cold deciduous forest (class 2 in Plate 3) for March and December. This point will be further discussed in section 4.4.

For all frequencies the general trend with increasing biomass density is an increase in horizontal polarization emissivity coupled with a decrease in polarization difference. For all vegetation classes, emissivities in both polarizations decrease with increasing frequency, although this trend is clearer for sparsely vegetated areas. The amplitude of the annual cycle, on average, is rather small, whatever the vegetation type. For the rain forest straddling the equator the annual pattern is the same for both hemispheres: The polarization dif-

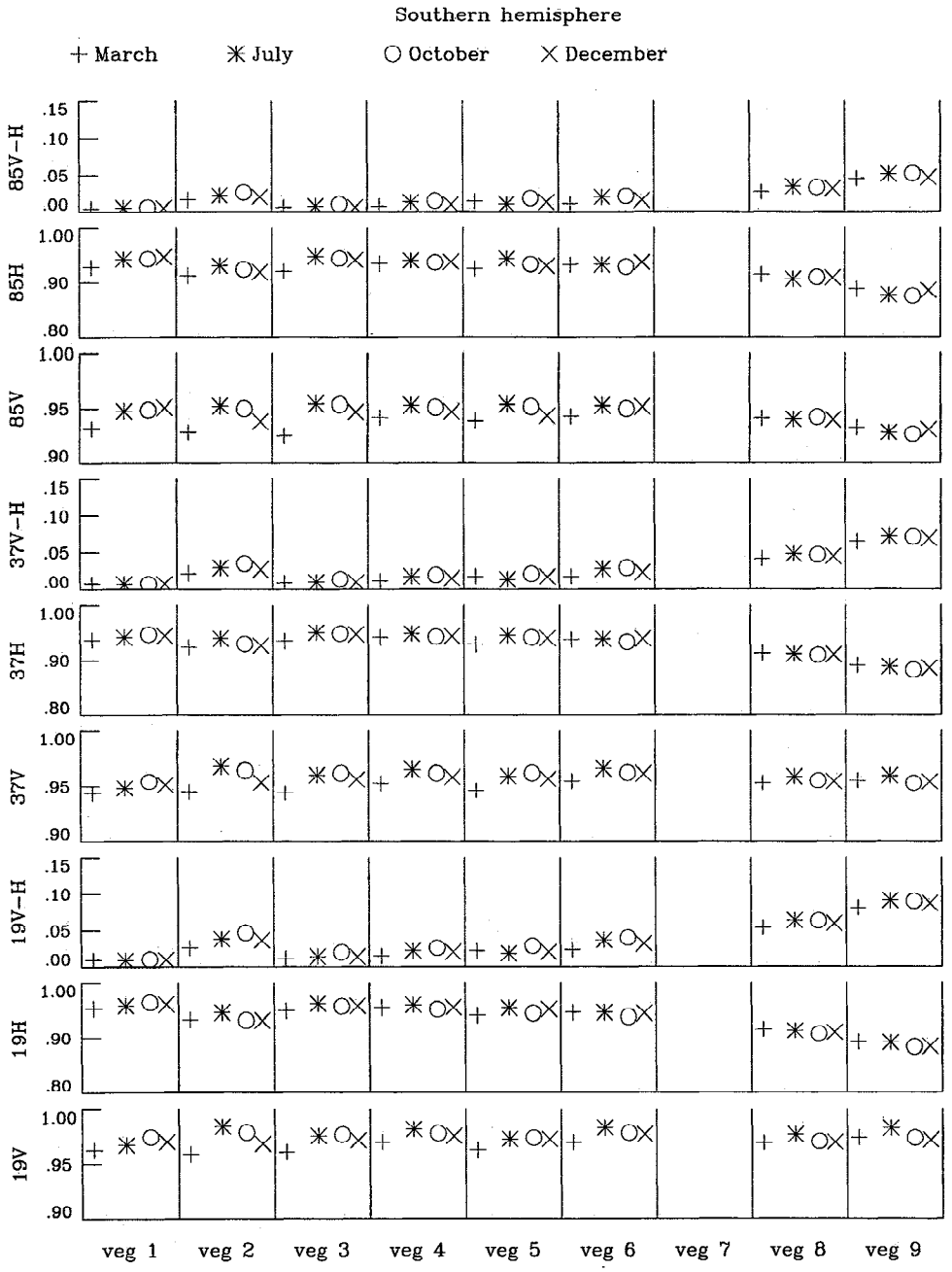

Figure 8b. Variations of the mean value of the emissivity at 19, 37, and 85 GHz (for both polarizations and difference in polarizations) for the four studied months and for the 10 vegetation types. Results are presented for the southern hemisphere.

ference is constant over the year but with a decrease in emissivities for all frequencies and polarizations in March. This feature seems to be related to an extension of the grassland-like area southwards during this month. For grasslands (class 4) and deciduous woodlands (class 6), differences in polarization show a slight annual cycle, which is opposite for the two hemispheres, as expected: The polarization differences decrease during the summer months as compared to the winter season. Although the seasonal cycle is rather weak, its amplitude depends on the vegetation type and could be further exploited for vegetation classification.

4.3. Monitoring of Inundated Areas and Sensitivity to Soil Moisture

Microwave observations have been shown to be valuable for delineating flooded areas [*Choudhury*, 1989; *Giddings and Choudhury*, 1989; *Neale et al.*, 1990; *Achutuni et al.*, 1996]. For instance, examination of the major river basins in South America with 37 GHz observations [*Giddings and Choudhury*, 1989] has shown that all major hydrological features, including wetlands and seasonal lakes, have a microwave signature at 37 GHz. The NOAA experimental soil and wetness index

(SWI), based on the observation of $TbH85 - TbH19$, is now used as guidance to monitor flooding on a global basis [*Achutuni et al.*, 1996]. But flooding begins in periods of heavy rainfall that are also periods of maximum contamination of microwave radiances by clouds and rainfall. As shown in Figure 2, the number of SSM/I clear sky observations during the rainy season in Africa is very low, and caution should be exercised when using these indices.

In the microwave, flooding produces a decrease in emissivity in both polarizations but an increase in the polarization differences, especially at lower frequencies, because of the differences in dielectric properties of water and soil or vegetation. On the emissivity maps (Plate 4) the main hydrological features are delineated when their dimensions are comparable with the spatial resolution of the microwave satellite instruments. For instance, the Congo river appears clearly on the 19 GHz maps (Plate 1a and 4), especially in Zaire, where the river is wide and surrounded by swamps. Changes in the seasonal extent of the swamps are apparent between the rainy and dry months. In March, evidence of the western part of the river does not even appear in the retrieved 19 GHz emissivities because of the limited dimension of the river at that time of the year compared to the instrument field of view. Seasonal variations of some hydrological features are especially striking. In western Zambia, for instance, around 13°S and 22°E, a large flooded area apparent in March after the rainy season completely disappears in July and October and reappears to a limited extent in December. The Zambezi river that flows in this region is associated with seasonal swamps. We extracted monthly mean precipitation rates for this region from the GPCP (Global Precipitation Climatology Project) gridded rain gauge data set [*Huffman et al.*, 1996]. These data show good agreement with the extension of the Zambezi swamps. Figure 9 shows the emissivity in western Zambia for March and October 1991 at 19, 37, and 85 GHz for both polarizations, along with the monthly precipitation in this region for the same year. In Sudan, swamps related to the White Nile (around 9°N and 29°E) also exhibit seasonal variations associated with the rainy season: While unobservable in March after the dry season, the extent of the flooding increases from July to a maximum in December. Another large seasonal feature can be observed in Namibia around 19°S and 16°E (the Etosha pan). In Mali the swamps connected to the Niger River show a seasonal cycle in the horizontal emissivity, although this wetland is situated in an arid region where the horizontal emissivity of the dry soil is already low.

Although the microwave emissivity is known to be sensitive to soil wetness [*Schmugge et al.*, 1980, 1989; *Wang et al.*, 1983; *Ulaby et al.*, 1983; *Hallikainen et al.*, 1985; *Owe and Chang*, 1988; *Felde*, 1996], soil roughness and particularly the presence of vegetation pose serious problems in the detection of soil moisture variations. In the present study the sensitivity of the retrieved emissivity to soil moisture has not been investigated in de-

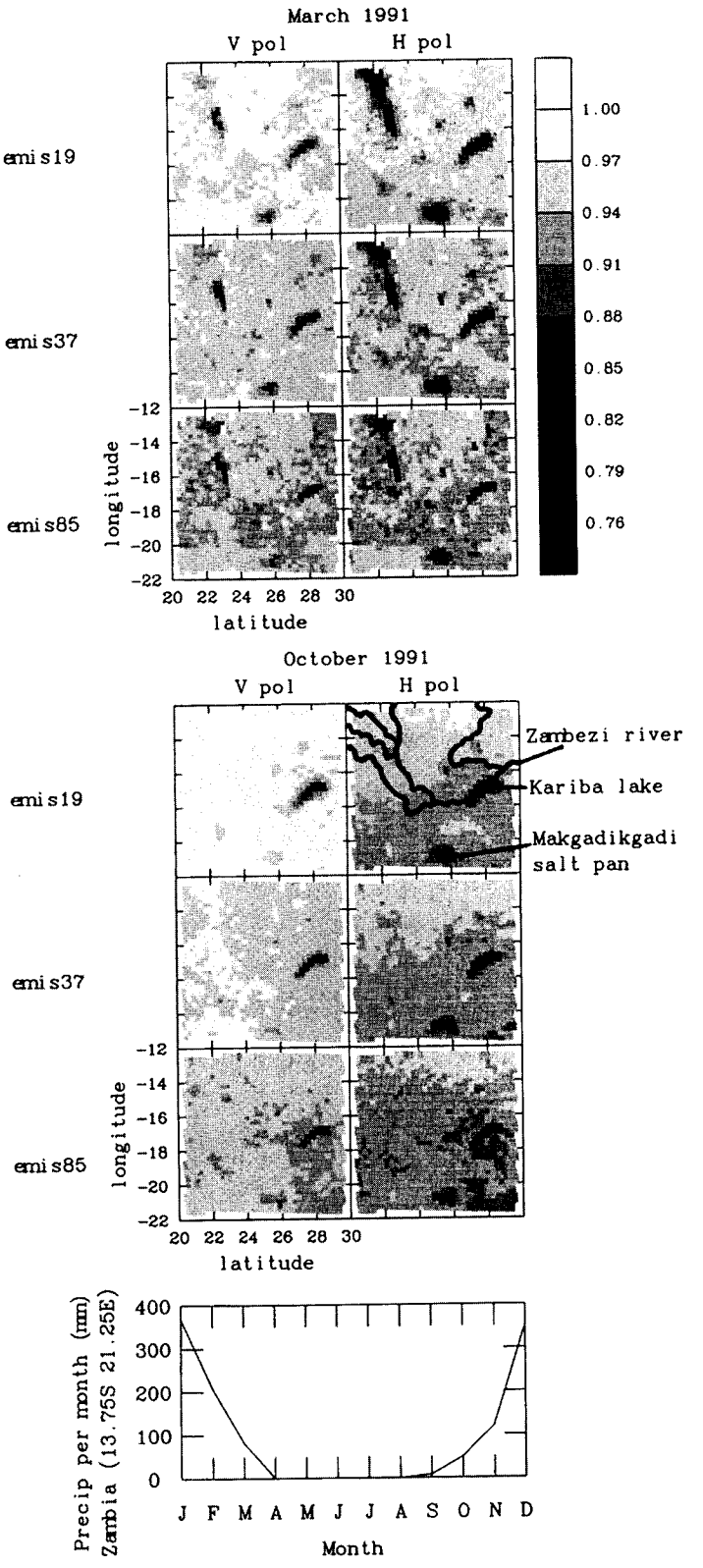

Figure 9. Surface emissivities in western Zambia for March and October 1991 at 19, 37, and 85GHz for both polarizations. In October for the 19 GHz H polarization, the main hydrological features are added. The monthly precipitation (in millimeter) for this year is also shown for the same area.

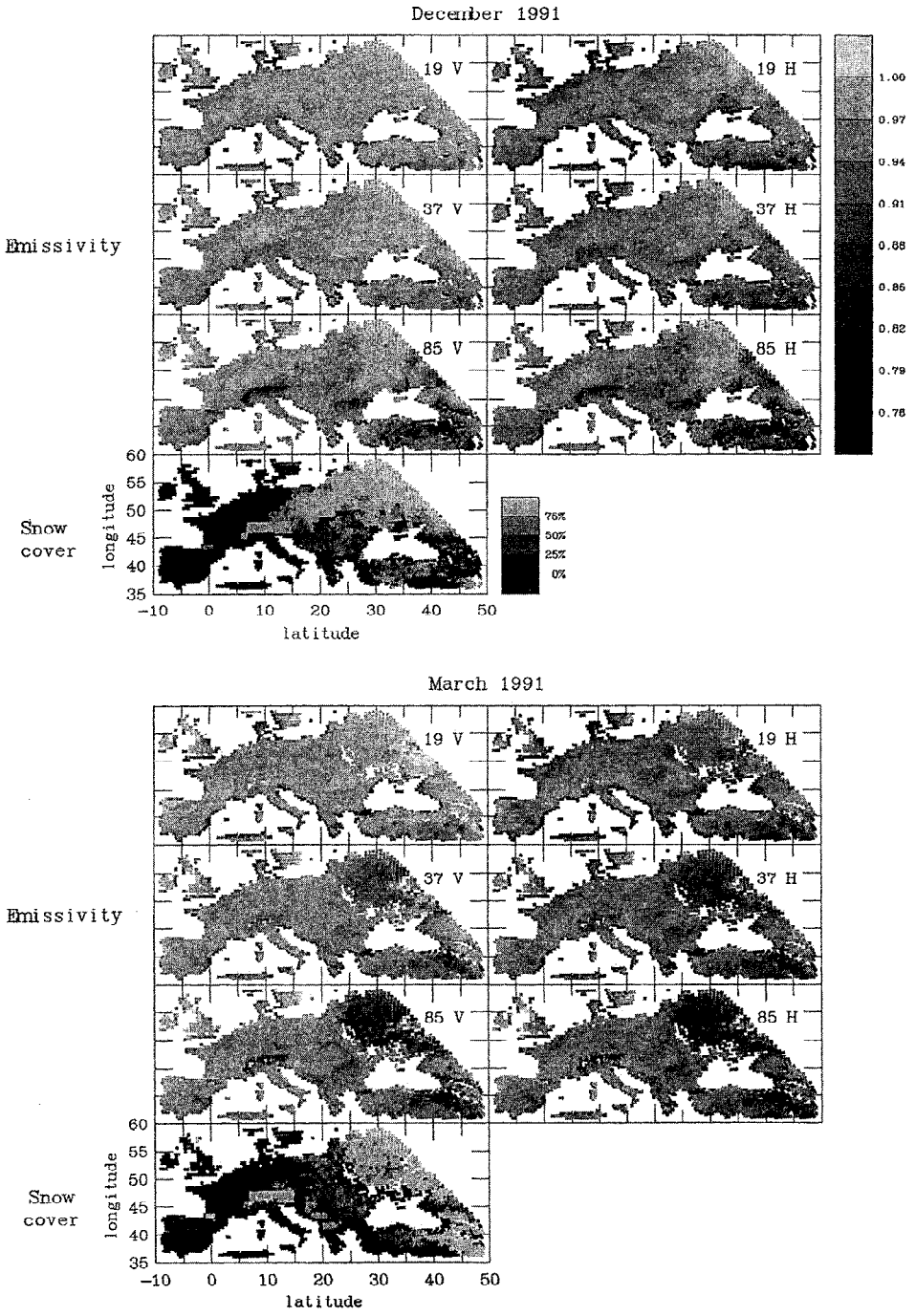

Figure 10. Emissivity maps of part of Europe at 19, 37, and 85 GHz (both polarizations) for December and March 1991. The percentage of snow cover pixels during a month is also presented for these 2 months.

tail, for instance, with the help of AIP (antecedent precipitation index) [*Wilke and McFarland*, 1986]. There is one notable feature that may be related to soil moisture: On the 19 GHz emissivity maps (Plates 1a and 4) northwestern Europe (northern France, United Kingdom and Belgium) exhibits a decreased emissivity for both polarizations from July, October, and December to March, with a corresponding increase in polarization difference. This signature is not seen in surrounding areas with similar vegetation types. Similar features are apparent at 37 and 85 GHz, but the trend is weaker at the higher frequencies. Correlative data are needed to confirm that this feature is related to soil moisture, but these maritime regions are very humid from fall to spring under the influence of marine air.

4.4. Snow Effects

In December and March in eastern Europe and western Asia, the 19 GHz emissivity shows a pattern that is probably related to the presence of snow (Plate 4). For

the region north of 35°N, the retrieved emissivities are displayed for 19, 37, and 85 GHz at both polarizations (Figure 0). Also presented is the snow cover defined for each location as the number of fully snow covered pixels processed during the month divided by the total number of SSM/I pixels processed for that month at that location. The snow cover information is from the NOAA operational analysis (as reported in the ISCCP data set). In December, extensive snow cover correlates with higher emissivity for all frequencies and polarizations, except at 37 and 85 GHz in areas of high elevation (the Alps, the Transylvanian Alps, the Caucasus mountains). Whatever the frequency, polarization differences (not presented here) do not show any special signature that correlates with the presence of snow. However, a very different behavior prevails in March. At 37 and 85 GHz the snow cover is associated with a decline of the emissivities at both vertical and horizontal polarizations, while the emissivity at 19 GHz vertical polarization is higher than in the snow-free areas, and the 19 GHz horizontal polarization is equivalent to the snow-free emissivities in adjacent regions. Polarization differences decline with the presence of snow; the lower the frequency, the stronger this effect. At 85 GHz this feature is not apparent. At this time of the year, the emissivity behavior does not depend primarily on the topography. At 85 GHz, high standard deviations for the months of December and March are associated with snow covered pixels; this is not the case at 19 GHz.

The substantially different behavior of the snow emissivities for these 2 months may be explained by differences in the snow physical properties. We analyzed relationships between emissivities and surface temperatures, but no correlation was found; however, we did not look for lagged correlations. Because in situ measurements of snow parameters such as wetness or depth are scarce and not readily available, we have not yet examined them. Nonetheless, a short overview of the microwave response to snow can help interpret the retrieved emissivity values.

A snowpack can consist of several layers having different densities and crystal-size distributions. The properties of these layers reflect the snowpack's history and usually relate to location and elevation. Microwave radiation penetrates the snow and responds to snowpack properties such as depth, melting, refreezing, and embedded vegetation. The penetration of the microwave radiation also means that the IR skin temperature may differ from the effective microwave emission temperature of the snow pack, adding to the variability of the retrieved microwave emissivity. Large differences in the dielectric properties of liquid and frozen water at microwave frequencies yield substantial variations of the snow emissivity with wetness and melting. The dielectric constant of dry snow varies between 1 (air) and 3.2 (ice), depending on the density of the snow and shape of the grains. As a consequence, the dielectric losses in dry snow are very small, and the extinction coefficient is dominated by scattering. Volume scattering by individual ice grain reduces the emitted radiation. The scattering effect is stronger at shorter wavelengths and for larger particles and drier snow. Because water has a much higher dielectric constant, variations in snow wetness produce large changes in snow emissivity: With increasing wetness the dielectric losses become large and the scattering negligible. Wet snowpacks radiate like black bodies at the physical temperature of the snow layer. In the spring, prior to runoff, the snow undergoes melting and refreezing cycles during which large spherical grains are formed. The microwave signature of the snowpack then varies between characteristics for wet snow to high reflectivities due to strong volume scattering by the large inhomogeneities. Although a number of studies have focused on mapping snow cover and properties from microwave observations [e.g., *Kunzi et al.*, 1984; *Chang et al.*, 1987; *Hall et al.*, 1991; *Grody and Basist*, 1996], the microwave signature of snow, highly variable in time and space, is not well understood. Thorough reviews of the snow microwave signature are provided by *Ulaby et al.* [1983] and *Foster et al.*, [1984].

In the light of this brief review, a tentative interpretation of the retrieved emissivities is proposed. In December at lower elevation there is no sign of scattering by snow: Wet snow (high emissivity, higher than the surrounding snow-free areas) covers part of eastern Europe. The mountains are covered with dry snow that produces scattering at high frequencies (lower emissivities). In March, regardless of the topography of the snow-covered regions, the 37 and 85 GHz frequencies exhibit scattering in the snowpack (low emissivities), while the 19 GHz does not (higher emissivities). We suspect that the snow is dry enough to permit scattering at higher frequencies, but that the inhomogeneities are not large enough to scatter much 19 GHz radiation. To better understand the observed signatures and to interpret the day-to-day variations observed in the snow emissivity, analysis of the depositional history of snowfall and associated meteorological conditions is required.

5. Conclusions and Possibilities

Microwave emissivities of the land surface are estimated from SSM/I observations by removing contributions from the atmosphere, clouds and rain using ancillary satellite data from ISCCP and TOVS. The microwave emissivities have been calculated for Africa, large parts of Europe, and western Asia for March, July, October, and December 1991. Correspondences between geographical patterns and seasonal variations of the microwave emissivities with variations in vegetation, flooded areas and snow cover have been analyzed. In the absence of direct measurements of surface emissivities at these larger spatial scales, these comparisons show that the regional patterns and seasonal changes of the retrieved emissivities are compatible with large-scale topography and vegetation distributions and with flooding and snow cover events. The standard deviations of the day-to-day variations of the emissivities

are typically about 0.012 for all the channels. Higher standard deviations, especially over the desert, are related to significant and probably spurious standard deviations of the water vapor amounts reported by the TOVS analysis in these areas. The strong diurnal cycle in these regions, in conjunction with the use of only one TOVS profile, may also contribute to this feature. Overall, the low standard deviations set an upper limit on the errors in retrieving land surface emissivities with this technique, ~0.02.

The feasibility of estimating accurate microwave emissivities over land offers a number of interesting possibilities for their use in atmospheric and cloud parameter retrievals and monitoring the land surface itself. We briefly review here the potential uses of these products.

With accurate estimates of land microwave emissivities (and surface skin temperature), it is possible to consider extending atmospheric and cloud property retrievals from microwave measurements developed over ocean to land areas. A sensitivity study can tell which parameters can be retrieved with acceptable accuracy and will help in selecting an adequate retrieval method. Figures 11 and 12 present the sensitivity of the SSM/I observations to changes in water vapor column abundance (WV) and cloud liquid water path (LWP) along with the sensitivity of the resulting WV and LWP to errors in the estimated emissivities. As shown in these figures, the higher the emissivity, the lower the sensitivity to WV and LWP as expected. The 22 and 85 GHz channels are the most sensitive to water vapor,

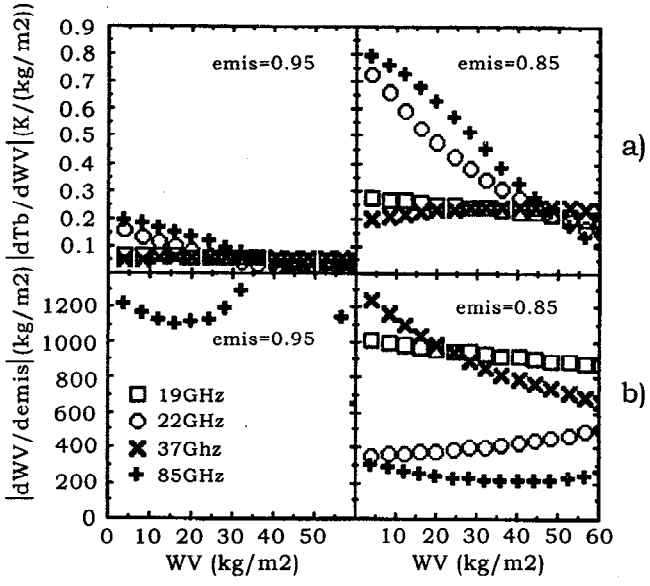

Figure 11. (a) Sensitivity of the SSM/I Tbs to changes in the water vapor content (WV) in K per kg/m^2. (b) For a given SSM/I brightness temperature, sensitivity of the corresponding WV to changes in surface emissivities, in kg/m^2 per unit emissivity. The simulations are presented for a tropical atmospheric profile and a surface temperature of 299 K. The water vapor content of the tropical atmosphere is scaled to fit the given water vapor content. Two surface emissivities are selected: 0.95 and 0.85.

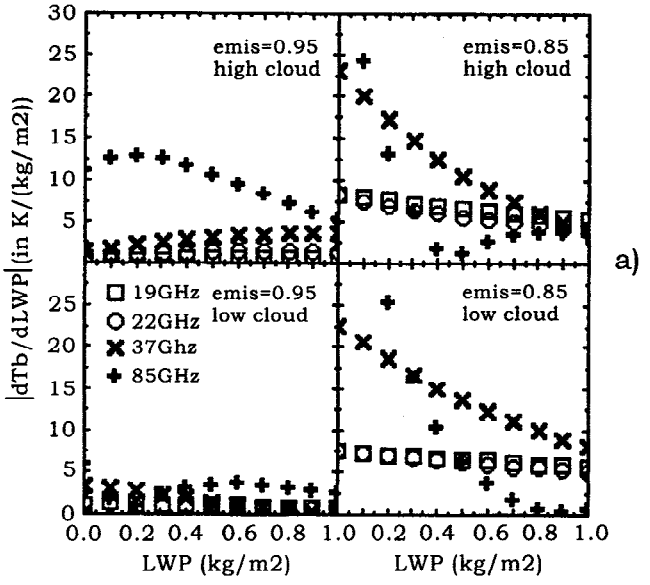

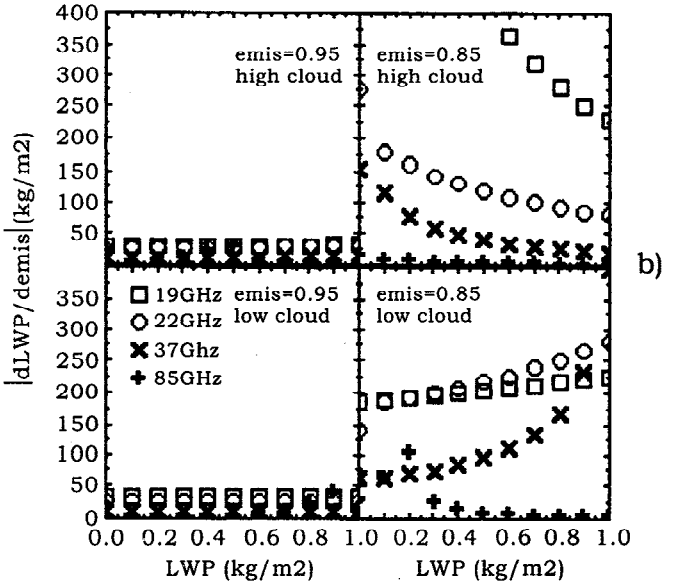

Figure 12. (a) Sensitivity of the SSM/I Tbs to changes in cloud liquid water contents, in K per kg/m^2. (b) For a given SSM/I brightness temperature, sensitivity of the corresponding liquid water path to changes in the surface emissivity, in kg/m^2 per unit emissivity. The results are presented for two land emissivities (0.95 and 0.85) and two cloud types (high cloud from 650 to 585 mbar with a mean temperature of 262 K; low cloud from 800 to 725 mbar with a mean temperature of 273 K). A U. S. Standard atmosphere is selected, with a water vapor content of 14.3 kg/m^2 and a surface temperature of 287 K.

but for high surface emissivities (>0.95), the sensitivity of Tb to WV does not exceed 0.2 K per kg/m^2. As a consequence, one cannot expect an accurate retrieval of the water vapor content from SSM/I over densely vegetated areas where emissivities are ~0.95 for both H and V polarizations. When land emissivities are lower, for

example, over the desert for the H polarization, the sensitivity of the 85 GHz channel to WV is much higher. However, as a consequence of this high sensitivity to WV, the emissivity retrievals in these areas and at this frequency are more sensitive to errors in the water vapor data set used, as evidenced by the rather large standard deviations for a month (as high as 0.04). Considering the impact of errors in the WV for a given error in emissivity (~200 kg/m^2 per unit change in emissivity, see Figure 11b), the accuracy of the WV retrieval will be low. However, an iterative approach exploiting the different WV sensitivities of the SSM/I channels may be possible.

For LWP the sensitivity of the SSM/I *Tbs* increases with increasing frequency and shows dramatic variations with cloud parameters and surface emissivities. The ability to estimate LWP essentially depends on the contrast between the radiance emitted by the cloud and the radiance that emanates from the surface. As a result, the accuracy of a potential LWP retrieval will depend strongly on the cloud and surface conditions. The 85 GHz channel exhibits higher sensitivity to LWP, especially for low liquid water content but has a very nonlinear behavior. The 37 GHz channel, although less sensitive, shows a smoother behavior. Future work will involve the development of a variational inversion method to retrieve the LWP from the SSM/I observations above land. Such a process has already been adopted over ocean [*Phalippou*, 1996, *Prigent et al.*, 1997]. This method is based on nonlinear optimal estimation theory and will make use of the a priori information from TOVS (atmospheric profile), ISCCP (surface temperature, LWP, and cloud top temperature), and the surface emissivity estimates.

Given the weak frequency dependence of the emissivities, an estimate of the emissivities at AMSU frequencies could be interpolated from the estimated SSM/I emissivities, on a monthly basis, assuming a given angular dependence of the emissivities. The use of these emissivities in the advanced-TOVS (A-TOVS) process will enhance the accuracy of the lower atmospheric temperature retrieval.

Analysis of the correspondences between the microwave emissivities and vegetation distributions suggests the possibility of using microwave emissivities to monitor vegetation phenology at regional and continental scale. Although it may not be possible to discriminate between a large number of vegetation classes with microwave emissivities alone, spatial variations of these emissivities are well correlated with transitions in vegetation classes as defined by *Matthews* [1983] and may help refine information about the spatial distribution in land surface types, especially with respect to biomass density. In addition, discriminating among a larger number of vegetation classes may be possible when analyzing the seasonal variations of the microwave emissivity. Responding to different parameters of the vegetation, comparisons of the microwave emissivities with visible/IR reflectance are also very promising. Satellite observations at 0.6 μm are sensitive to the chlorophyll absorption and this property has been used to monitor the vegetation through the NDVI (normalized vegetation index as derived from optical and visible AVHRR data). Comparisons of MVI and NDVI have already been undertaken [*Becker and Choudhury*, 1988; *Tucker*, 1989; *Townshend et al.*, 1989a, b; *Justice et al.*, 1989]. However, the MVI is contaminated by surface temperature variations and cloud and atmosphere effects, as we have shown. In addition, the NDVI products contain contamination by clouds, aerosols and instrumental calibration [*Schlultz and Halpert*, 1995; *Rondeaux et al.*, 1996; *Gutman and Ignatov*, 1995], and the NOAA NDVI products [*Tarpley et al.*, 1984] are not yet available for 1991. Complementarity of the retrieved microwave emissivities and optical parameters have to be examined.

The SSM/I land emissivities show a strong sensitivity to flooding and snow and could be used to monitor these conditions. However, for these applications, shorter time composites of the emissivities should be considered, although these events are usually associated with significant cloudiness. Since a large proportion of inundated pixels are within the intertropical cloud region, these results indicate that the 19 GHz could be used for flood monitoring, and the stringent constraint on cloud cover could be relaxed because of the lower sensitivity of the 19 GHz channel to clouds. On the other hand, for snow monitoring the sensitivity of each channel to snow parameters makes it difficult to tolerate more clouds without degradation of the retrieval at higher frequencies. Both of these tasks benefit from combining SSM/I with another satellite data set, like ISCCP, that is more sensitive to clouds.

Future research should include radiative transfer modeling of the various land surfaces and comparisons with retrieved emissivities to further understand the complex physics of surface emissivities, possibly to invert the radiative transfer equation to retrieve soil and vegetation parameters [*Calvet et al.*, 1994, 1996].

Acknowledgment. The authors are grateful to Alison Walker for her help in processing the ISCCP data sets.

References

Achutuni, R., R. A. Scofield, N. C. Grody and C. Tsai, Global monitoring of large area flooding using the DMSP SSM/I soil wetness index, paper presented at Annual Meeting, American Meteorol. Soc., Atlanta, Ga., 1996.

Becker, F. and B. J. Choudhury, Relative sensitivity of normalized difference vegetation index (NDVI) and microwave polarization difference index (MPDI) for vegetation and desertification monitoring, *Remote Sens. Environ.*, 24, 297-311, 1988.

Calvet, J. C., J. P. Wigneron, E. Mougin, Y. H. Kerr and J. L. Brito, Plant water content and temperature of the Amazon forest from satellite microwave radiometry, *IEEE Trans. Geosci. Remote Sens.*, 32, 397-407, 1994.

Calvet, J. F., A. Chanzy and J. P. Wigneron, Surface temperature and soil moisture retrieval in the Sahel from airborne multifrequency microwave radiometry, *IEEE Trans. Geosci. Remote Sens.*, 34, 588-599, 1996.

Chang, A. T. C., J. L. Foster and D. K. Hall, Nimbus-7

SMMR derived global snow cover parameter, *Ann. Glaciol.*, 9, 39-44, 1987.

Choudhury, B. J., Monitoring global land surface using Nimbus-7 37GHz data. Theory and examples, *Int. J. Remote Sens.*, 10, 1579-1605, 1989.

Choudhury, B. J., Microwave vegetation index: a new long-term global data set for biospheric studies, *Int. J. Remote Sens.*, 9, 185-186, 1988.

Choudhury, B. J., Reflectivities of selected land surface types at 19 and 37GHz from SSM/I observations, *Remote Sens. Environ.*, 46, 1-17, 1993.

Choudhury, B. J. and C. J. Tucker, Monitoring global vegetation using Nimbus-7 37GHz data. Some empirical relations, *Int. J. Remote Sens.*, 8, 1085-1090, 1987.

Conner, M. D. and G. W. Petty, SSM/I brightness temperature deviations from gridded monthly means as a basis for over-land precipitation estimation, paper presented at Annual Meeting, Am. Meteorol. Soc., Atlanta, Ga., 1996.

English, S. J., C. Guillou, C. Prigent and P. J. Jones, Aircraft measurements of water vapour continuum absorption at millimetre wavelength, *Q. J. R. Meteorol. Soc.*, 120, 603-625, 1994.

Felde, G. W., The effect of soil moisture on a passive microwave vegetation index, paper presented at Annual Meeting, Am. Meteorol. Soc., Atlanta, Ga., 1996.

Foster, J. L., D. K. Hall and A. T. C. Chang, An overview of passive microwave snow research and results, *Rev. Geophys.*, 22, 195-208, 1984.

Giddings, L.and B. J. Choudhury, Observation of hydrological feature with Nimbus-7 37GHz data applied to South America, *Int. J. Remote Sens.*, 10, 1673-1686, 1989.

Grody, N. C. and A. N. Basist, Global identification of snow cover using SSM/I measurements, *IEEE Trans. Geosci. Remote Sens.*, 34, 237-249, 1996.

Gutman, G.and A. Ignatov, Global land monitoring from AVHRR: potential and limitation, *Int. J. Remote Sens.*, 16, 2301-2309, 1995.

Hall, D. K., M. Sturm, C. S. Benson, A. T. C. Chang, J. L. Foster, H. Garbeil and E. Chacho, Passive Microwave Remote sensing and in situ measurements of Arctic and Subarctic snow, *Remote Sens. Environ.*, 38, 161-172, 1991.

Hall, F. G., K. F. Huemmrich, S. J. Goetz, P. J. Sellers and J. E. Nickelson, Satellite remote sensing of surface energy balance: Success, failure, and unresolved issues in FIRE, *J. Geophys. Res.*, 97, 19061-19089, 1992.

Hallikainen, M., F. T. Ulaby, M. C. Dobson, M. El-Rayes and L. K. Wu, Microwave dielectric behavior of wet soil. Part 1: empirical models and experimental observations, *IEEE Trans. Geosci. Remote Sens.*, 23, 25-34, 1985.

Han, Y., J. Snider and E. R. Westwater, Observations of water vapor by ground based microwave radiometers and Raman lidar, *J. Geophys. Res.*, 101, 3775-3788, 1994.

Hollinger, J. P., R. Lo, G. Poe, R. Savage and J. Pierce, Special Sensor Microwave/Imager user's guide, Nav. Res. Lab. Washington, D. C., 1987.

Hollinger, J. P., J. L. Pierce and G. A. Poe, SSM/I instrument evaluation, *IEEE Trans. Geosci. Remote Sens.*, 28, 781-790, 1990.

Huffman, G. J., GPCP version 1 combined precipitation data set, SSAI, Lab. for Atmos., Natl. Aeronaut. and Space. Admin., Goddard Space Flight Cent., Greenbelt, Md., 1996.

Jin, Y., W. B. Rossow and D. P. Wylie, Comparison of the climatologies of high-level clouds from HIRS and ISCCP, *J. Clim.*, 9, 2850-2879, 1996.

Jones, A. S. and H. T. Vonder Haar, Passive microwave remote sensing of cloud liquid water over land regions, *J. Geophys. Res.*, 95, 16673-16683, 1990.

Justice, C. O., J. R. Townshend and B. J. Choudhury, Comparison of AVHRR and SMMR data for monitoring vegetation phenology on a continental scale, *Int. J. Remote Sens.*, 10, 1607-1632, 1989.

Kerr, Y. H. and E. G. Njoku, On the use of passive microwave at 37GHz in remote sensing of vegetation, *Int. J. Remote Sens.*, 14, 1931-1943, 1993.

Kunzi, K. F., S. Patil and H. Rott, Snow cover parameters retrieved from Nimbus-7 scanning multichannel microwave radiometer (SMMR) data, *IEEE Trans. Geosci. Remote Sens.*, 20, 452-467, 1984.

Liebe, H. J., G. A. Hufford and M. G. Cotton, Propagation modeling of moist air and suspended water/ice particles at frequencies below 1000GHz, paper presented at Specialist Meeting of the Electromagnetic Wave Propagation Panel, Adv. Group for Aerosp. Res. and Dev., Palma de Mallorca, Spain, 1993.

Lin, B. and W. B. Rossow, Observations of cloud liquid water path over oceans: optical and microwave remote sensing methods, *J. Geophys. Res.*, 99, 20907-20927, 1994.

Matthews, E., Global vegetation and land use: new high-resolution data bases for climate studies, *J. Clim. Appl. Meteorol.*, 22, 474-486, 1983.

Matthews, E. and W. B. Rossow, Regional and seasonal variations of surface reflectance from satellite observations at 0.6microns, *J. Clim. Appl. Meteorol.*, 26, 170-202, 1987.

Matzler, C., Seasonal evolution of microwave radiation from an oat field, *Remote Sens. Environ.*, 31, 161-173, 1990.

Neale, C. M., M. J. McFarland and K. Chang, Land surface-type classification using microwave temperatures from the Special Sensor Microwave /Imager, *IEEE Trans. Geosci. Remote Sens.*, 28, 829-838, 1990.

Ottle, C. and M. Stoll, Effect of atmopsheric absorption and surface emissivity on the determination of land surface temperature from infrared satellite data, *Int. J. Remote Sens.*, 14, 2025-2037, 1993.

Owe, M., A. Chang and R. E. Golus, Estimating surface soil moisture from satellite microwave measurements and a satellite derived vegetation index, *Remote Sens. Environ.*, 24, 331-345, 1988.

Phalippou, L., Variational retrieval of humidity profile, wind speed and cloud liquid water path with SSM/I: Potential for numerical weather prediction, *Q. J. R. Meteorol. Soc.*, 122, 327-355, 1988.

Prigent, C., L. Phalippou and S. English, Variational inversion of SSM/I observations during the ASTEX campaign, *J. Appl. Meteorol.*, 36, 493-508, 1997.

Prince, S. D. and B. J. Choudhury, Interpretation of Nimbus-7 37GHz microwave brightness temperature data in semi-arid southern Africa, *Int. J. Remote Sens.*, 10, 1643-1661, 1989.

Rondeaux, G., M. Steven and F. Baret, Optimization of soil-adjusted vegetation indices, *Remote Sens. Environ.*, 55, 97-107, 1989.

Rossow, W. B. and L. C. Garder, Cloud detection using satellite measurements of infrared and visible radiances for ISCCP, *J. Clim.*, 6, 2341-2369, 1993a.

Rossow, W. B. and L. C. Garder, Validation of ISCCP cloud detections, *J. Clim.*, 6, 2370-2393, 1993b.

Rossow, W. B. and R. A. Schiffer, ISCCP cloud data products, *Bull. Am. Meteorol. Soc.*, 72, 2-20, 1991.

Rossow, W. B., C. L. Brest and L. C. Garder, Global, seasonal surface variations from satellite radiance measurements, *J. Clim.*, 2, 214-247, 1989.

Rossow, W. B., A. W. Walker, D. E. Beuschel and M. D. Roiter, International Satellite Cloud Climatology Project (ISCCP): Document on new cloud datasets, Natl. Aeronaut. ans Space Admin., Goddard Institute for Space Stud., New York, N. Y., 1996.

Salisbury, J. W. and D. M. D'Aria, Emissivity of terrestrial materials in the 8-14μm atmospheric window, *Remote Sens. Environ.*, 42, 83-106, 1992a.

Salisbury, J. W. and D. M. D'Aria, Infrared (8-14μm) remote sensing of soil particle size, *Remote Sens. Environ.*, 42, 157-165, 1992b.

Schlultz, P. A. and M. S. Halpert, Global analysis of the relationships among a vegetation index, precipitation and land surface temperature, *Int. J. Remote Sens.*, 16, 2755-2777, 1995.

Schmugge, T. J., T. J. Jackson and H. K. McKim, Survey of method for soil moisture determination, *Water Resour. Res.*, 16, 961-979, 1980.

Schmugge, T., P. E. O'Neill and J. R. Wang, Passive microwave soil moisture research, *IEEE Trans. Geosci. Remote Sens.*, 24, 12-22, 1989.

Snider, J. B., D. A. Hazen, A. J. Francavilla, W. B. Madsen and M. D. Jacobson, Comparison of observed and theoretical millimeter wave absorption: Implication for remote sensing of atmospheric water, paper presented at International Geoscience and Remote Sensing Symposium 95, Florence, Italy, 1995.

Tarpley, J. D., S. R. Schneider and R. L Money, Global vegetation indices from the NOAA-7 Meteorological Satellite, *J. Clim. Appl. Meteorol.*, 23, 491-494, 1984.

Townshend, J. R. G., C. O. Justice, B. J. Choudury, C. J. Tucker, V. T. Kalb and T. E. Goff, A comparison of SMMR and AVHRR data for continental land cover characterization, *Int. J. Remote Sens.*, 10, 1633-1642, 1989a.

Townshend, J. R. G., B. J. Choudhury, L. Giddings, O. Justice, S. D. Prince and C. J. Tucker, Comparison of data from the scanning multifrequency microwave radiometer (SMRR) with data from the advanced very high resolution radiometer (AVHRR) for terrestrial environmental monitoring: An overview, *Int. J. Remote Sens.*, 10, 1687-1690, 1989b.

Tucker, C. J., Comparing SMMR and AVHRR data for drought monitoring, *Int. J. Remote Sens.*, 10, 1663-1672, 1989.

Tucker, C. J., Relating SMMR 37GHz polarization difference to precipitation and atmospheric carbon dioxide concentration: A reappraisal, *Int. J. Remote Sens.*, 13, 177-191, 1992.

Ulaby, F. T. and W. H. Stiles, The active and passive response to snow parameters. Part 1: Water equivalent of dry snow, *J. Geophys. Res.*, 85, 1045-1049, 1980.

Ulaby, F. T., M. Razani and M. C. Dobson, Effects of vegetation cover on the microwave radiometric sensitivity to soil moisture, *IEEE Trans. Geosci. Remote Sens.*, 21, 51-61, 1983.

Ulaby, F. T., R. K. Moore and A. K. Fung, *Microwave Remote Sensing, Active and Passive*, vol. 3, Artech House, Reading, Ma., 1986.

Wang, J. R., Effect of vegetation on soil moisture sensing observed from orbiting microwave radiometers, *Remote Sens. Environ.*, 17, 141-151, 1985.

Wang, J. R., P. E. O'Neill, T. J. Jackson and E. T. Engman, Multifrequency measurements of the effects of soil moisture, soil texture and surface roughness, *IEEE Trans. Geosci. Remote Sens.*, 21, 44-51, 1983.

Weng, F. and N. Grody, Retrieval of liquid and ice water in the atmosphere using Special Sensor Microwave Imager (SSM/I) data, *J. Geophys. Res.*, 99, 25535-25551, 1994.

Wentz, F. J., User's manual SSM/I antenna temperature tapes, RSS Tech. Rep. 032588, Remote Sens. Syst., Santa Rosa, Calif., 1988.

Wilke, G. D. and M. J. McFarland, Correlations between Nimbus-7 scanning multichannel microwave radiometer and an Antecedent Precipitation Index, *J. Clim. Appl. Meteorol.*, 25, 227-238, 1986.

C. Prigent and W. B. Rossow, NASA Goddard Institute for Space Studies, 2880 Broadway, New York, N.Y. 10025 e-mail: cprigent@giss.nasa.gov

E. Matthews, Center for Climate System Research, Columbia University, NASA Goddard Institute for Space Studies, 2880 Broadway,New York, N.Y. 10025 e-mail: cprigent@giss.nasa.gov

(Received December 24, 1996; revised March 21, 1997; accepted May 2, 1997 .)